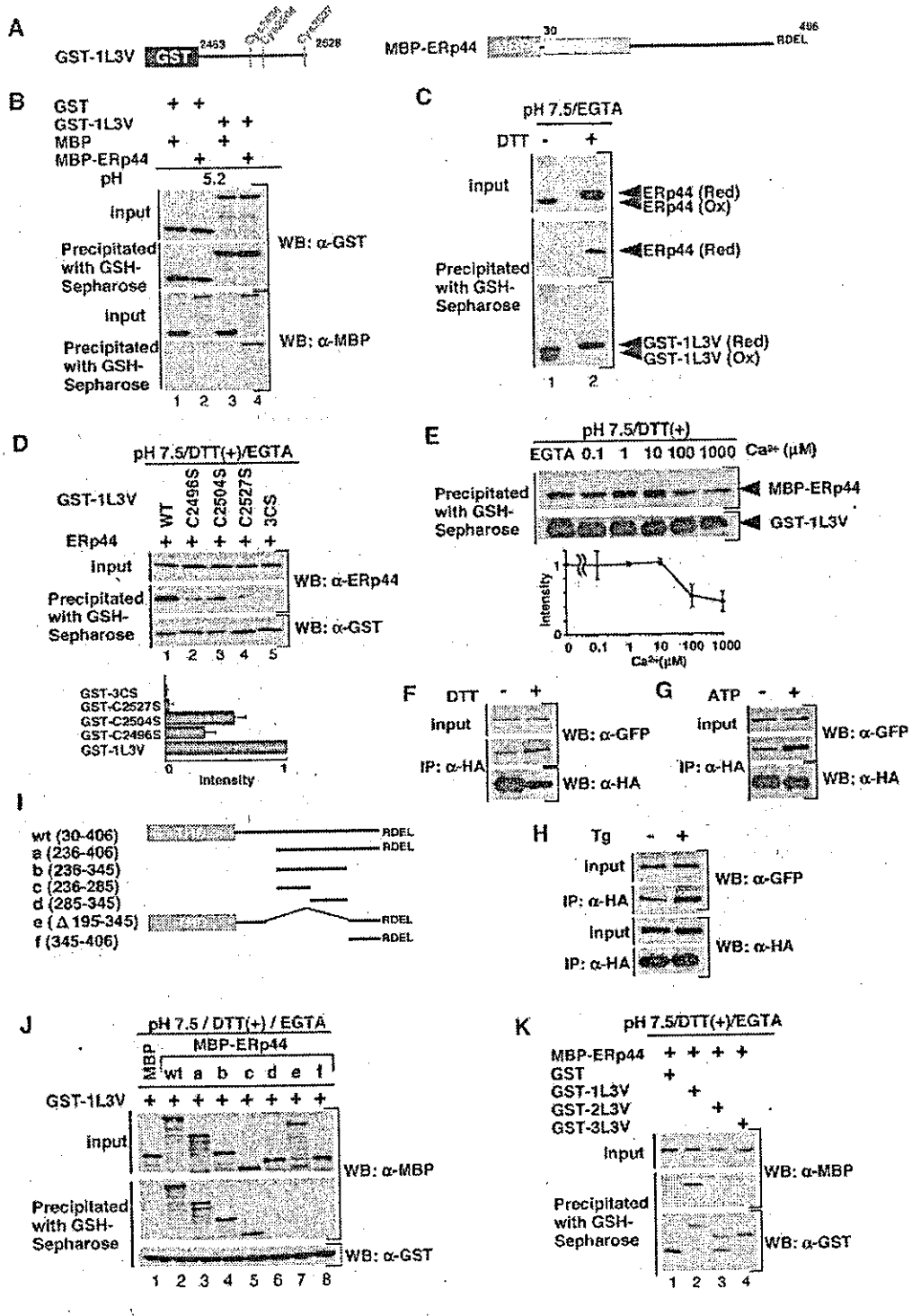

Figure 2. ERp44 Specifically Interacts with IP_3R1 in a Condition-Dependent Manner

(A) Schematic representation of recombinant proteins.

(B) ERp44 directly interacts with 1L3V in acidic buffer. Purified GST (lanes 1 and 2) or GST-1L3V (lanes 3 and 4) was incubated with purified MBP (lanes 1 and 3) or MBP-ERp44 (lanes 2 and 4) in acidic solution (pH 5.2) containing 4 mM Ca^{2+} and then precipitated with GSH-Sepharose. Precipitated proteins were subjected to Western blotting with α-GST or α-MBP.

(C) ERp44 directly interacts with 1L3V in the presence of DTT and EGTA in neutral buffer. To obtain untagged ERp44, purified GST-ERp44

region of ERp44 by fusing the full-length (without the signal sequence) or subfragments of ERp44 to MBP and testing their interactions with GST-1L3V in the presence of DTT at neutral pH. Wild-type MBP-ERp44 and MBP-ERp44 (the C-terminal half) strongly interacted with GST-1L3V (Figure 2J, lanes 2 and 3, respectively), indicating that THD is not required for the interaction. MBP-ERp44c, which contains a highly conserved glutamate-rich region but is devoid of the histidine-rich region, also bound to GST-1L3V, albeit somewhat weakly (Figure 2J, lane 5), whereas other mutants tested did not (Figure 2J, lanes 6–8). These results indicate amino acid residues 236–285 of ERp44 to be necessary and sufficient for binding to 1L3V. The primary sequence of this region has no similarities to any sequences in the database but is well conserved among species (Supplemental Figure S3 on the *Cell* website).

Finally, MBP-ERp44 interacted with GST-1L3V, but not with GST-2L3V or GST-3L3V (Figure 2K), which is consistent with the results of the initial screening with L3V-Fc and the IP experiment (Figures 1C and 1F, respectively). Based on all of the above findings, it was concluded that ERp44 directly interacts with the L3V domain of IP_3R1 in a subtype-specific and ER lumenal environment-dependent manner.

Expression of ERp44 Inhibits IICR via IP_3R1

To explore the functional consequences of ERp44 binding to IP_3R1, we performed Ca^{2+}-imaging experiments with the fluorescent Ca^{2+} indicator fura-2. First, we tested HeLa cells, approximately half of whose IP_3Rs are IP_3R1 (Hattori et al., 2004). Red fluorescent protein (RFP)-tagged ERp44 (RFP-ERp44) or RFP with an ER retention signal (RFP-RDEL, negative control) was then expressed in HeLa cells, and the cells were stimulated with ATP in Ca^{2+}-free medium. In nonexpressing cells, ATP (3 μM) typically caused a single Ca^{2+} transient, occasionally with small oscillations (Figure 3A, black trace), and the response of the cells expressing RFP-RDEL was indistinguishable from that of the nonexpressing cells (Figure 3A, red trace). Cells expressing RFP-ERp44, on the other hand, typically exhibited significantly smaller Ca^{2+} transients (Figure 3B, red trace), and the average peak amplitude in cells expressing RFP-ERp44 was significantly smaller (69.3% ± 1.8%, $p < 0.05$) than that in the nonexpressing cells (Figure 3C). The difference was not due to a decrease in releasable Ca^{2+} in the ER because the amount of the passive Ca^{2+} leakage elicited by Tg was unchanged (Figures 3D and 3E). Also, IP_3 production was not influenced by overexpression of ERp44 (data not shown).

Next, we tested the effect of ERp44 overexpression in COS-7 cells because they are known to express no IP_3R1 (Boehning and Joseph, 2000; Hattori et al., 2004). Stimulation of cells expressing RFP-RDEL with 1 μM ATP typically elicited a single Ca^{2+} transient (Figure 3F), while expression of RFP-ERp44 had no effect on the pattern or amplitude of the transient (Figures 3G and 3H). No effect of RFP-ERp44 expression was observed when cells were stimulated with lower ATP concentrations (0.3 μM) (data not shown).

The above results suggest that ERp44 inhibits IP_3R1 but does not inhibit IP_3R2 or IP_3R3. To further confirm this, we needed to compare cells that express IP_3R1 only to those expressing no IP_3R1. This was achieved by employing DT40-KMN60 and DT40-1KO cells, both of which were derived from the same parent cell line, DT40 cells. The DT40-KMN60 cell line was established by stably transfecting the mouse IP_3R1 gene on a background of IP_3R-deficient DT40 cells (DT40-TKO, Sugawara et al., 1997). DT40-1KO cells express IP_3R2 and IP_3R3, but not IP_3R1 (Sugawara et al., 1997). Crosslinking of the B cell antigen receptor (BCR) activates PLC-γ, which results in production of IP_3 in DT40 cells. The peak amplitude of BCR-induced Ca^{2+} release in DT40-KMN60 cells expressing RFP-RDEL was approximately the same (96% ± 2.9%) as in nonexpressing cells (Figure 3K), but it was significantly smaller in DT40-KMN60 cells expressing RFP-ERp44 (60.6% ± 9.6%, Figures 3I and 3K). There was no reduction in Tg-induced Ca^{2+} leakage

---

was cleaved by thrombin and the GST released then was removed by incubation with GSH-Sepharose. This ERp44 protein was incubated with GST-1L3V in neutral solution (pH 7.5) containing 5 mM EGTA in the presence or absence of 3 mM DTT. The inputs and bead bound proteins were resolved with SDS-PAGE under nonreducing conditions and analyzed by Western blotting with α-ERp44 (top and middle) or α-GST (bottom).

(D) Purified GST-1L3V (lane 1) and its cysteine mutants, C2496S (lane 2), C2504S (lane 3), C2527S (lane 4), and 3CS (C2496S/C2504S/C2527S, lane 5), were incubated with ERp44 (as prepared in [C]) in the presence of 3 mM DTT and 5 mM EGTA. Proteins were then precipitated with GSH-Sepharose and subjected to Western blotting with α-ERp44 (middle) or α-GST (bottom). The amount of ERp44 added to the binding reaction is shown at the top. The histogram depicts densitometric analyses from five independent experiments.

(E) Ca^{2+} dependency of the interaction between 1L3V with ERp44. A binding assay was performed with 3 mM DTT in the presence of EGTA or the Ca^{2+} concentration indicated. Proteins bound to GSH-Sepharose were subjected to Western blotting with α-MBP (top) or α-GST (bottom).

(F) In vivo interaction between IP_3R1 and ERp44 is enhanced under reducing conditions. COS-7 cells expressing GFP-IP_3R1 and HA-ERp44 were treated with 5 mM DTT for 30 min (+) or not (–), then treated with DSP, and IP was performed. The lysates and IP samples were analyzed by Western blotting with α-GFP (top and middle) or α-HA (bottom).

(G and H) In vivo interaction between IP_3R1 and ERp44 is enhanced after ER Ca^{2+} depletion. COS-7 cells expressing GFP-IP_3R1 and HA-ERp44 were stimulated with 10 μM ATP (+) or not (–) for 5 min (G), or 2 μM Tg (+) or not (–) for 30 min (H), treated with DSP, and finally IP was performed. The lysates and IP samples were analyzed by Western blotting with α-GFP or α-HA.

(I) Schematic representation of ERp44 and its mutants.

(J) Amino acid residues 236–285 of ERp44 are responsible for interaction with 1L3V. GST-1L3V was incubated with MBP (lane 1) or MBP fusion proteins containing subfragments of ERp44 (lanes 2–8). Binding assay was performed as in (E). The "control" MBP protein (lane 1) is in fact MBP plus 94 unrelated amino acids derived from the vector (pMAL-c) sequence and its molecular weight is thus larger than those of some ERp44-fusion proteins.

(K) ERp44 specifically interacts with the L3V of IP_3R1, but not that of IP_3R2 or IP_3R3. Purified GST (lane 1), GST-1L3V (lane 2), GST-2L3V (lane 3), or GST-3L3V (lane 4) was incubated with MBP-ERp44 in neutral solution (pH 7.5) containing EGTA and DTT. Proteins bound to GSH-Sepharose were subjected to Western blotting with α-MBP (top and middle) or α-GST (bottom).

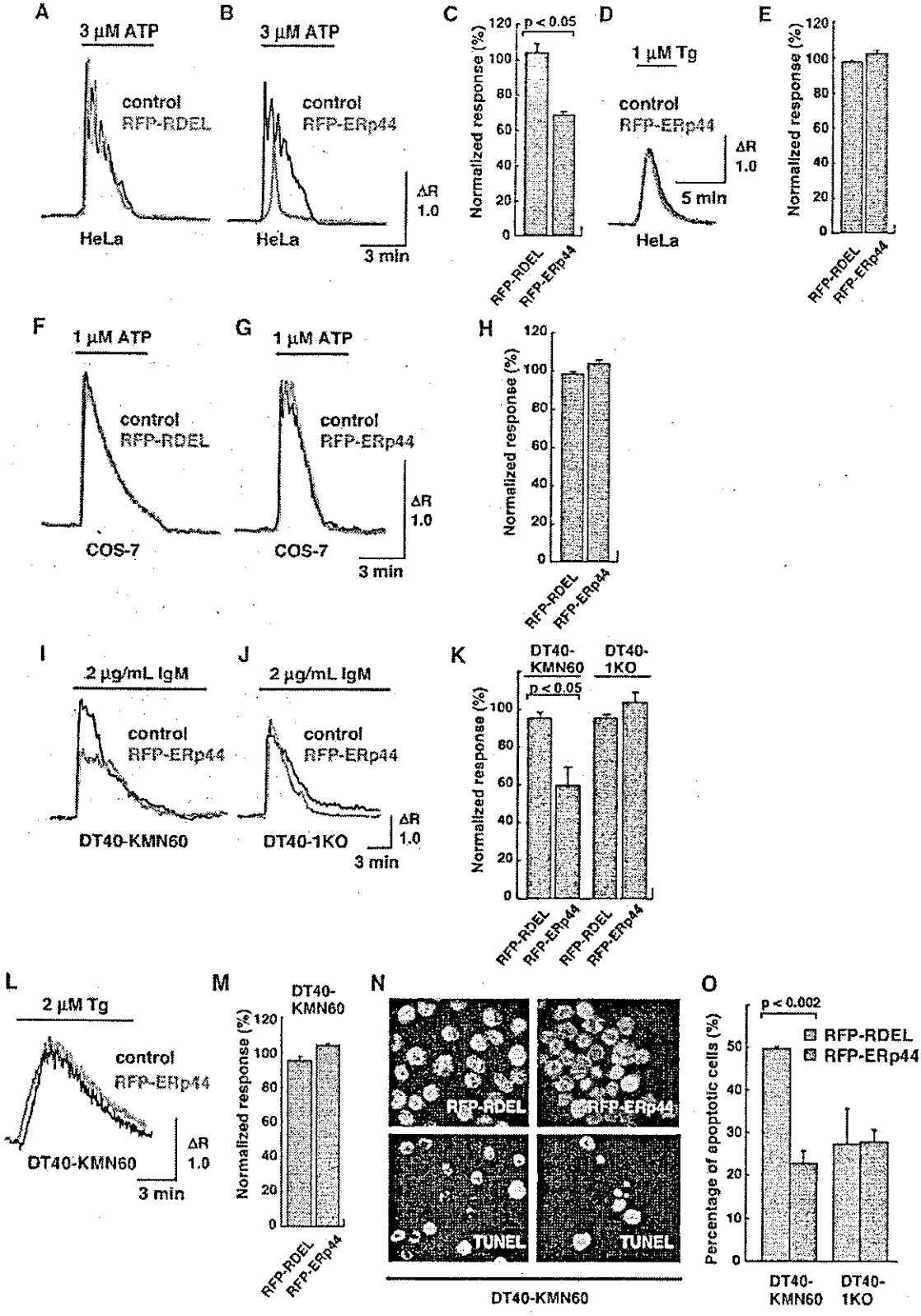
A
3 μM ATP
control
RFP-RDEL
HeLa
B
3 μM ATP
control
RFP-ERp44
HeLa
ΔR
1.0
3 min
C
p < 0.05
Normalized response (%)
RFP-RDEL
RFP-ERp44
D
1 μM Tg
control
RFP-ERp44
ΔR
1.0
5 min
HeLa
E
Normalized response (%)
RFP-RDEL
RFP-ERp44
F
1 μM ATP
control
RFP-RDEL
COS-7
G
1 μM ATP
control
RFP-ERp44
COS-7
ΔR
1.0
3 min
H
Normalized response (%)
RFP-RDEL
RFP-ERp44
I
2 μg/mL IgM
control
RFP-ERp44
DT40-KMN60
J
2 μg/mL IgM
control
RFP-ERp44
DT40-1KO
ΔR
1.0
3 min
K
DT40-KMN60
DT40-1KO
p < 0.05
Normalized response (%)
RFP-RDEL
RFP-ERp44
RFP-RDEL
RFP-ERp44
L
2 μM Tg
control
RFP-ERp44
DT40-KMN60
ΔR
1.0
3 min
M
DT40-KMN60
Normalized response (%)
RFP-RDEL
RFP-ERp44
N
RFP-RDEL
RFP-ERp44
TUNEL
TUNEL
DT40-KMN60
O
p < 0.002
RFP-RDEL
RFP-ERp44
Percentage of apoptotic cells (%)
DT40-KMN60
DT40-1KO

in these cells (Figures 3L and 3M). In DT40-1KO cells, on the other hand, expression of RFP-ERp44 had little effect on the peak amplitude (Figures 3J and 3K). These results indicate that ERp44 inhibits IP_3R1, but not IP_3R2 or IP_3R3.

IP_3Rs have a critical function in BCR-induced apoptosis in DT40 cells (Sugawara et al., 1997). We found that expression of REP-ERp44, but not RFP-RDEL, significantly inhibited apoptosis in DT40-KMN60 cells (Figures 3N and 3O), but no such effect was observed in DT40-1KO cells (Figure 3O), implying that inhibition of IP_3R1 by ERp44 affects cell functions, such as apoptosis.

Specific Knockdown of ERp44 Results in Augmentation of IICR via IP_3R1

Next, we used the RNA interference technique to investigate the role of endogenous ERp44 by testing two different small interfering RNA (siRNA) sequences targeted to the open reading frame (siERp44-ORF) and the 3′-untranslated region (siERp44-3U), respectively, of human ERp44. To provide negative controls, we introduced three-point mutations in these siRNAs (siControl-ORF or siControl-3U, respectively). Western analysis revealed both siERp44-ORF and siERp44-3U to efficiently and specifically "knock down" ERp44 in HeLa and COS-7 cells (Figure 4A). Unfortunately, however, none of the siRNAs targeted to chicken ERp44 decreased the amount of ERp44 in DT40 cells (data not shown). In HeLa cells, knockdown of ERp44 neither affected the expression of other ER oxidoreductases nor induced unfolded protein response within 48 hr (Supplemental Figure S5 online).

SiRNA-transfected HeLa cells were stimulated with 1, 3, and 10 μM ATP. Stimulation with 1 μM ATP rarely (4.0% ± 0.3% of all cells) evoked discernible Ca^{2+} signals in siControl-3U-transfected cells (Figures 4B and 4C, black trace and bar), whereas approximately five times the number (20.1% ± 2.5%) of siERp44-3U-transfected cells responded (Figures 4B and 4C, red trace and bar). Subsequent stimulation with 3 μM ATP elicited IICR in 46.9% ± 1.6% of the control cells and 90.3% ± 1.2% of the cells transfected with siERp44-3U (Figures 4B and 4C), whereas most of the cells in both preparations responded when stimulated with 10 μM ATP (Figure 4C). The average peak amplitude was higher in siERp44-3U-transfected cells than in the siControl-3U-transfected cells at all ATP concentrations (Figure 4D). These ERp44 knockdown effects were confirmed to be specific by transfecting the cells with RFP-ERp44 ("rescue" experiments, Supplemental Figure S4). Knockdown of ERp44 had no effect on the Ca^{2+} leakage induced by Tg (data not shown).

We then performed the same experiments in COS-7 cells. Since COS-7 cells do not express IP_3R1, we predicted that knockdown of ERp44 would have no effect on IICR in this cell line, and the results confirmed our prediction (Figures 4E–4G). These findings indicate that ERp44 specifically inhibits IP_3R1.

Cysteine Residues in the L3V Domain Are Important for Inhibition of IP_3R1 Activity by ERp44

Next, we investigated the significance of the cysteine residue(s) in 1L3V in terms of the inhibition of IP_3R1 by ERp44. We first investigated whether mutations of these residues in full-length (and GFP-tagged) IP_3R1 affected IICR activity (Figure 5A). When Cys2527, which is located adjacent to the channel pore region, was mutated, channel activity was completely lost (Figure 5A), and this mutant was not used any further. Mutations in Cys2496 and Cys2504, however, had no effect on channel activity (Figure 5A). Interaction between these IP_3R1 mutants and ERp44 was significantly decreased (Figure 5B), consistent with the results obtained with recombinant proteins (Figure 2D). The IP_3R1 mutant was cotransfected into DT40-TKO cells with either RFP-RDEL or RFP-ERp44, and a Ca^{2+}-imaging experiment was performed. IICR via GFP-IP_3R1 (i.e., wild-type) was suppressed by coexpression with RFP-ERp44, but not with RFP-RDEL (Figures 5C and 5F). Surprisingly, this inhibition by ERp44 was almost completely abolished by substitution of the Cys2496 or Cys2504 of GFP-IP_3R1 (Figures 5D and 5E, respectively, and Figure 5F). These results clearly demonstrated that the presence of free thiol groups in the L3V domain is important for inhibition of IP_3R1 by ERp44.

ERp44 Inactivates Channel Activity of IP_3R1 in Lipid-Bilayer System

To unambiguously demonstrate that ERp44 inhibits IP_3R1, we performed single-channel current recording

Figure 3. Expression of ERp44 Inhibits IICR in HeLa and DT40-KMN60 Cells, but Not in COS-7 or DT40-1KO Cells

(A and B) ERp44 inhibits IICR in HeLa cells. Cells transfected with either RFP-RDEL (A) or RFP-ERp44 (B) were stimulated with 3 μM ATP. Representative Ca^{2+} responses in nonexpressing (black) and expressing cells (red) are shown.

(C) Quantitation of results in (A) and (B). Normalized responses were calculated with the averaged peak amplitude of nonexpressing cells set equal to 100%. $p < 0.05$ compared to RFP-RDEL (Student's t test).

(D) The Ca^{2+} storage capacity is unchanged in HeLa cells expressing RFP-ERp44. Cells were stimulated with 1 μM Tg, and representative Ca^{2+} responses in nonexpressing (black) and expressing cells (red) are shown.

(E) Quantitation of the results in (D).

(F–H) ERp44 does not affect IICR in COS-7 cells. Cells transfected with either RFP-RDEL (F) or RFP-ERp44 (G) were stimulated with 1 μM ATP. Representative Ca^{2+} responses in nonexpressing (black) and expressing cells (red) are shown.

(H) Quantitation of results shown in (F) and (G).

(I–K) ERp44 inhibits IICR in DT40-KMN60 but not in DT40-1KO cells. Cells were stimulated with 2 μg/ml anti-IgM. Representative Ca^{2+} responses in nonexpressing (black) and expressing cells (red) are shown, and their quantitations are shown in (K).

(L and M) ERp44 does not affect Ca^{2+} storage capacity in DT40-KMN60 cells. Ca^{2+} responses in nonexpressing (black) and expressing cells (red) and their quantitations are shown in (M).

(N and O) ERp44 inhibits BCR-induced apoptosis in DT40-KMN60 cells, but not in DT40-1KO cells. Cells were treated with anti-IgM (2 μg/ml) for 24 hr and apoptosis was assessed by TUNEL assay. Data are TUNEL-positive cells as a percentage of all cells expressing RFP-RDEL (gray) or RFP-ERp44 (red) from two independent experiments. $p < 0.002$ compared with RFP-RDEL (Student's t test).

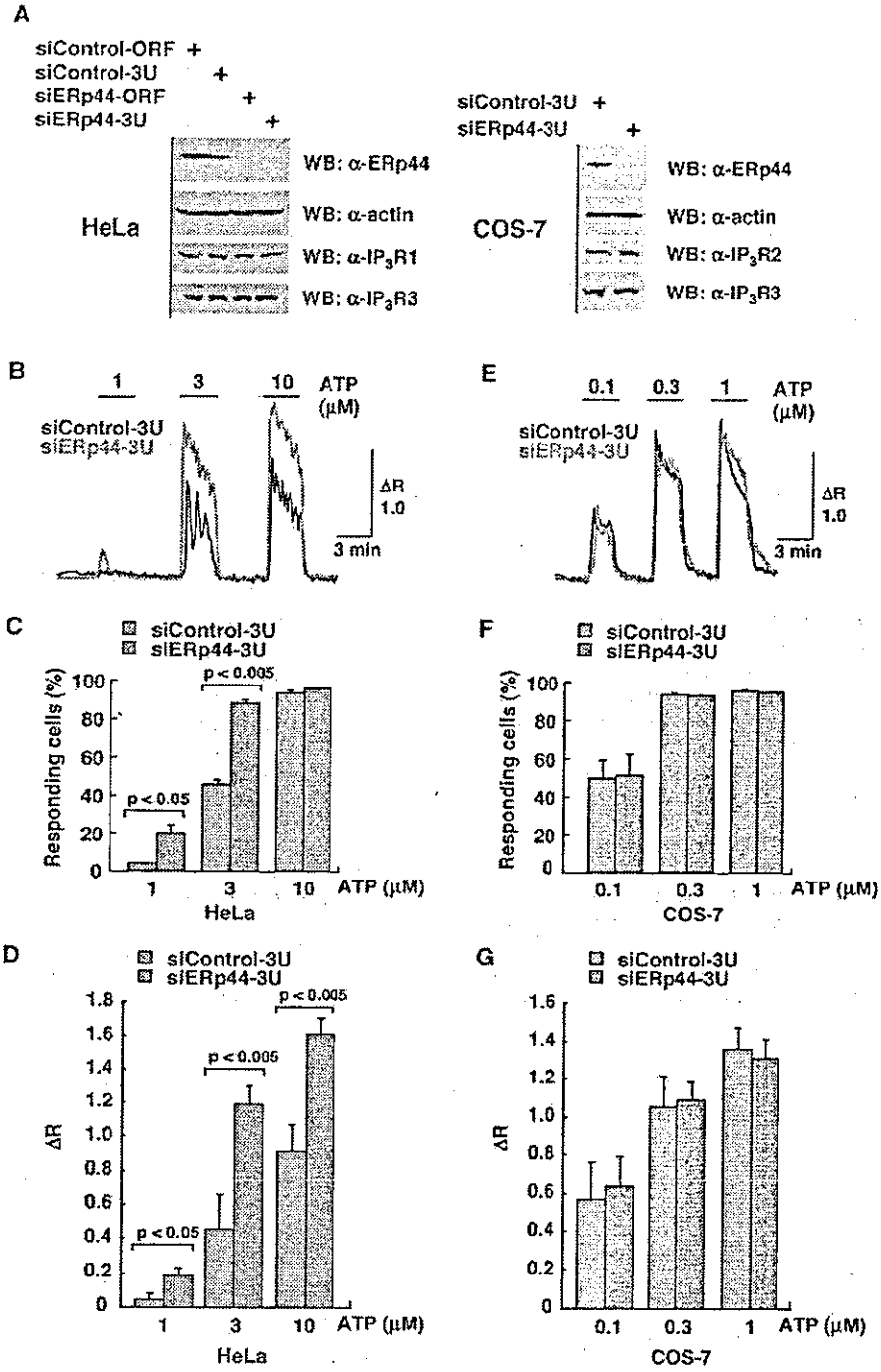

Figure 4. Knockdown of ERp44 Augments IICR in HeLa Cells, but Not in COS-7 Cells

(A) Knockdown of ERp44 in HeLa and COS-7 cells. The lysates of HeLa (left) and COS-7 cells (right) transfected with the siRNA indicated were analyzed by Western blotting with the antibodies indicated.

(B) Knockdown of ERp44 augments IICR in HeLa cells. Cells were stimulated with 1, 3, and 10 μM ATP in the presence of extracellular Ca^{2+}. Representative Ca^{2+} responses in siControl-3U-transfected (black) or siERp44-3U-transfected cells (red) are shown.

(C) Percentages of HeLa cells transfected with siControl-3U (gray) or siERp44-3U (red) that showed discernible Ca^{2+} responses at the ATP concentrations indicated.

(D) Average peak amplitude of the Ca^{2+} response in HeLa cells transfected with siControl-3U (gray) or siERp44-3U (red).

(E) COS-7 cells were stimulated with 0.1, 0.3, and 1 μM ATP in the presence of extracellular Ca^{2+}. Representative Ca^{2+} responses in siControl-3U-transfected (black) and siERp44-3U-transfected cells (red) are shown.

(F) Percentages of COS-7 cells transfected with siControl-3U (gray bars) or siERp44-3U (red bars) that showed discernible Ca^{2+} responses at the ATP concentrations indicated.

(G) Average peak amplitude of the Ca^{2+} response in COS-7 cells transfected with siControl-3U (gray columns) or siERp44-3U (red columns).

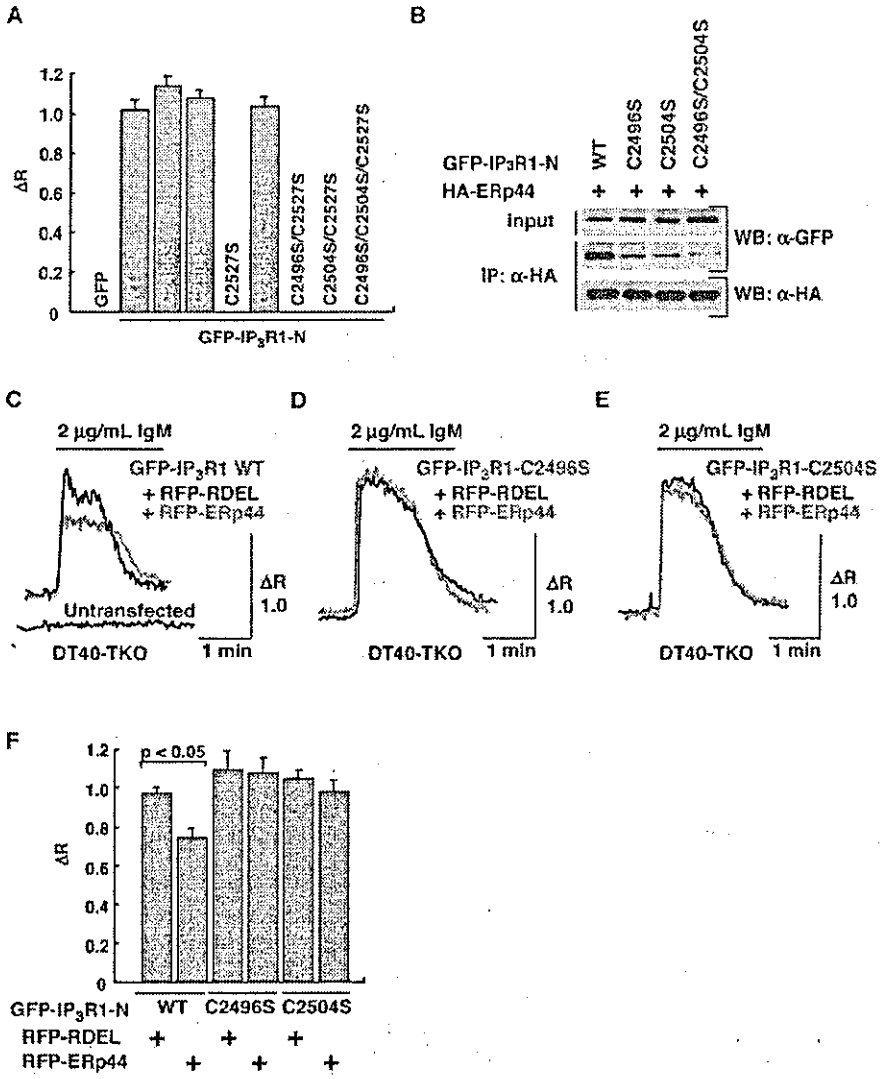

Figure 5. Cysteine Residues of 1L3V Are Required for Inhibition of IP_3R1 by ERp44

(A) DT40-TKO cells expressing GFP, GFP-IP_3R1, or GFP-IP_3R1 with cysteine replacements were stimulated with 2 μg/ml anti-IgM. Average peak amplitudes of the Ca^{2+} response are shown.

(B) Cysteine residues of the L3V domain of IP_3R1 are important for interaction between IP_3R1 and ERp44. GFP-IP_3R1 or its cysteine mutant was transfected with HA-ERp44 in COS-7 cells. Thirty-six hours after transfection, the cells were treated with DSP, and IP was performed with anti-HA. The lysates and IP samples were analyzed by Western blotting with α-GFP (top and middle) or α-HA (bottom).

(C–E) ERp44 inhibits IICR in DT40-TKO cells expressing IP_3R1, but not in cells expressing IP_3R1 cysteine mutants. RFP-RDEL or RFP-ERp44 was transfected into DT40-TKO cells with GFP-IP_3R1 or its cysteine mutant. Thirty-six hours after transfection, the cells were stimulated with 2 μg/ml anti-IgM. Representative Ca^{2+} responses in RFP-RDEL-expressing (black) and RFP-ERp44-expressing cells (red) are shown.

(F) Summary of the Ca^{2+}-imaging experiments in (C)–(E). Average peak amplitudes of the ratios are shown.

in a planar lipid bilayer fused with mouse cerebellar microsomes in which 99% of the IP_3Rs are IP_3R1 (Taylor et al., 1999). We first confirmed the interaction between MBP-ERp44 and GST-1L3V in the lumenal-side solution containing 3 mM DTT (Figure 6A). IP_3R1 activity was recorded with Ba^{2+} as a charge carrier in the presence of 3 mM DTT in the trans (lumenal) compartment. Addition of MBP-ERp44 resulted in inhibition of the channel activity in a dose-dependent manner (Figures 6B–6E), but addition of MBP (negative control) to the lumenal compartment had no effect on IP_3R1 activity (data not shown). Whether or not addition of more MBP-ERp44 can completely block the channel activity was not testable since we were unable to obtain a more concentrated recombinant ERp44 protein and adding more of the solution had nonspecific effects on channel activity (data not shown). ERp44 decreased the frequency of channel opening, but did not affect the mean open time of the channel (1.6 ± 0.5 ms and 1.5 ± 0.7 ms [mean ± SD, n = 6] before and after addition of 7.5 μM MBP-ERp44,

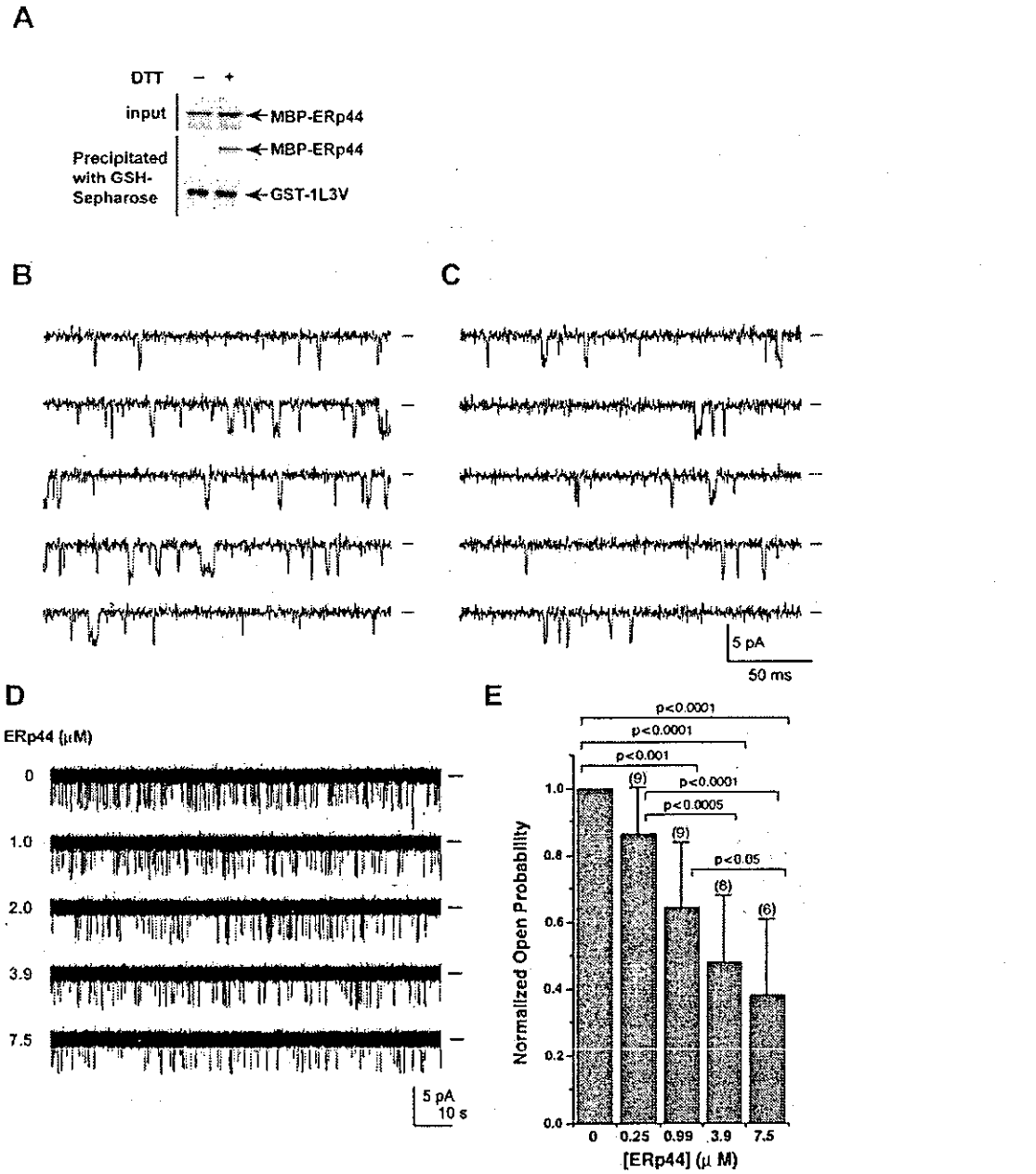

Figure 6. ERp44 Inhibits IP_3R1 in a Lipid Bilayer System

(A) MBP-ERp44 and GST-1L3V were incubated in the *trans* solution with (+) or without (–) 3 mM DTT and then precipitated with GSH-Sepharose. Precipitated proteins were analyzed by Western blotting.

(B and C) Sequential records before (B) and after addition (C) of 7.5 μM MBP-ERp44. Channels were recorded at −20 mV. Continuous 1 s records filtered at 1 kHz are shown.

(D) Effects of ERp44 on single-channel activity of IP_3R1 in the presence of 6.4 μM cytosolic (*cis*) IP_3 and 3 mM lumenal (*trans*) DTT. Serial additions of purified MBP-ERp44 were made to the lumenal compartment. Channel openings are shown as downward deflections from baseline (denoted by the horizontal lines). The data shown are representative of six independent experiments. Data were filtered at 0.5 kHz. The absolute values of open probability before the addition of ERp44 were in the 0.008–0.086 range.

(E) Dose-dependent inactivation of IP_3R1 by ERp44 under lumenal reducing conditions. The averages of open probabilities were normalized to the maximum IP_3R1 activity observed in each experiment. The data are means ± SD. Statistical analysis was done using repeated measures one-way ANOVA with Bonferoni's post-hoc tests. The number of independent trials is indicated above each bar.

respectively), indicating that ERp44 modulated the closed state of IP_3R1. Similarly, addition of ERp44 did not alter the amplitude of the single-channel current (3.7 ± 0.2 pA and 3.6 ± 0.2 pA [mean ± SD, n = 6] at −20 mV before versus after addition of MBP-ERp44, respectively). Raising the IP_3 concentration to 25 μM did not reverse the inhibitory effect of MBP-ERp44, and there was no indication that MBP-ERp44 lowers the IP_3 sensitivity of IP_3R1 (data not shown). No inactivation was observed in the absence of DTT (data not shown), further supporting the hypothesis that the free thiol group(s) in the L3V domain are involved in inhibition by ERp44. These bilayer studies revealed that ERp44 functions to maintain the closed state of IP_3R1 rather than affecting the characteristics of its open state.

Discussion

In this study we demonstrated that ERp44 directly interacts with the L3V domain of IP_3R1, thereby inhibiting its channel activity. This functional interaction is dependent on the pH, redox state, and $[Ca^{2+}]_{ER}$. It is particularly noteworthy that cysteine residues in the L3V domain of IP_3R1 play critical roles in both interaction with and inhibition by ERp44. This is the first example of a negative regulator of IP_3Rs on the ER lumen side and provides support for the hypothesis that IP_3Rs are specifically controlled by the intralumenal, in addition to by the cytosolic, environment.

Roles of Redox State, $[Ca^{2+}]_{ER}$, and pH in Dynamic Regulation of IP_3R by ERp44

It is widely accepted that the ER lumen is more oxidizing than the cytosol, and the ratio of reduced to oxidized glutathione in the ER lumen has been estimated to be from 3:1 to 1:1 (Hwang et al., 1992; Bass et al., 2003), suggesting that roughly 50%–75% of all lumenal cysteine residues are in the reduced (free thiol) form. However, it is also known that some proteins are either exclusively in the oxidized or the reduced state. While the mechanisms that control the redox state of extracellular proteins and ER oxidoreductases are being clarified (Sevier and Kaiser, 2002), how the redox state of other ER resident proteins (including IP_3Rs) is regulated is poorly understood. Our results indicate that the interaction between ERp44 and 1L3V weakens as the number of free thiol groups on 1L3V decreases (Figures 2D, 2F, and 5B). Therefore, if the cysteine residues of an IP_3R1 tetramer form a disulfide bond or are modified by, for example, nitrosylation, it would not bind to ERp44. Based on all of the evidence considered, we hypothesize that some of the cysteine residues in the L3V domain of IP_3R1 are in their free (reduced) form and that others have formed disulfide bonds or are modified. The disulfide bonds may be formed in the same polypeptide, between subunits, or with other molecules. IP_3R1 that have free cysteine residues in the L3V domain are subject to inhibition by ERp44. It must be pointed out that the number and approximate positions of cysteine residues are conserved in all IP_3R subtypes (Figure 1B), raising the possibility that forming a heterotetramer with these subtypes by disulfide bonds may be one way that the IP_3R1 polypeptide escapes inhibition. Whether the redox state, modification, or disulfide bond formation of these cysteine residues is controlled by a specific mechanism is a crucial and challenging question.

Previous studies have shown IICR to be diminished at low $[Ca^{2+}]_{ER}$, and this finding cannot be fully explained by the decreased Ca^{2+} concentration gradient across the ER membrane (e.g., Caroppo et al., 2003). Since the interaction between ERp44 and IP_3R1 is weaker when $[Ca^{2+}]_{ER}$ exceeds 100 μM (i.e., at resting levels, Figure 2E), it is tempting to speculate that the inhibition of IICR previously observed at low $[Ca^{2+}]_{ER}$ is due to enhanced binding of ERp44 to IP_3R1. More detailed investigation at both the cellular and the single-channel level is necessary to resolve this issue.

The pH in the ER lumen has been considered to be almost neutral and stable even during and after Ca^{2+} release (Foyouzi-Youssefi et al., 2000; Kim et al., 1998). However, it is also known that the pH in the lumen of the sarcoendoplasmic reticulum changes drastically after Ca^{2+} release (Kamp et al., 1998), and oligodendrocytes (glial cell type that have long and branched protrusions like neurons) have pH "microdomains," some of which could be below 6.5 (Ro and Carson, 2004). Thus, the pH in the ER lumen may also change in certain cell types or under certain conditions, and in such cases IP_3R1 may be more subject to inhibition by ERp44.

Physiological Significance of IP_3R1 Inhibition by ERp44

Central neurons express exclusively IP_3R1 (Taylor et al., 1999) and it is well known that localized Ca^{2+} release plays a variety of roles in these cell types (Berridge, 2002). In view of the fact that ERp44 can regulate IP_3R1 in a microenvironment-dependent manner, it is tempting to hypothesize that ERp44 is involved in the spatiotemporal regulation of localized Ca^{2+} release in neurons. Particularly, as both IICR and the redox state are involved in synaptic modulations (Inoue et al., 1998; Nishiyama et al., 2000; Knapp and Klann, 2002), ERp44 may also function in these processes. In addition, it was recently appreciated that some of the genetic abnormalities that cause neurodegenerative diseases augment IICR (Tang et al., 2003; Stutzmann et al., 2004), which may be the direct cause of neuronal death. Whether these IICR-activating mutations affect the function of ERp44, or even whether ERp44 can counteract them, are important pathological questions.

More generally, since the ER is the intersection of many signaling pathways (Berridge et al., 2003; Orrenius et al., 2003), inhibition of IP_3R1 by ERp44 may be involved in the feedback system by which information that has converged in the ER lumen is conveyed to the cytosol/nucleus in the form of $[Ca^{2+}]_C$. In other words, ERp44 translates the ER lumenal environment into a $[Ca^{2+}]_C$ by modulating IP_3R, and such a mechanism would allow the functions of the ER lumen (e.g., folding and glycosylation) and of the cytosol/nucleus (e.g., phosphorylation signaling and gene expression) to operate in a concerted matter.

Since the functions of many ER lumenal enzymes and chaperones are Ca^{2+} dependent, inhibition of Ca^{2+} release when the $[Ca^{2+}]_{ER}$ falls below the resting level would be consistent with maintaining their functions.

ERp44 was identified as a protein that forms mixed disulfide bonds with Ero1α, an ER oxidoreductase (Anelli et al., 2002), and it was shown to be involved in ER retention of Ero1α (Anelli et al., 2003). The functions of Ero1 family proteins are not fully understood, but since they play pivotal roles in oxidative protein folding (Tu and Weissman, 2002), ERp44 may play dual roles in protein folding: inhibiting Ca^{2+} release (which reinforces Ca^{2+}-dependent chaperones) by inactivating IP_3R1 and supporting disulfide bond formation by reinforcing the Ero1α/oxidoreductase system. The fact that ERp44 is induced during the unfolded protein responses (Anelli et al., 2002) fits well with this model.

Redox-Dependent Regulation of Cellular Ca^{2+} Signaling

It was very recently reported that SERCA 2b activity is modulated by CRT and ERp57, an ER lumenal oxidoreductase, in a $[Ca^{2+}]_{ER}$- and redox state-dependent manner (Li and Camacho, 2004). Since the pump activity of SERCA 2b is higher when thiol groups in its lumenal loop are reduced, when the ER lumenal environment shifts to the reducing condition, Ca^{2+} uptake by SERCA 2b should be enhanced (by ERp57) and Ca^{2+} release via IP_3R1 should be inhibited (by ERp44). In other words, SERCA 2b and IP_3R1 work together to increase $[Ca^{2+}]_{ER}$ under reducing conditions. This is reasonable since a reduced ER lumenal environment is unfavorable for protein folding and increasing $[Ca^{2+}]_{ER}$ benefits the function of the many chaperones and oxidoreductases that require a relatively high $[Ca^{2+}]_{ER}$. Finally, we obtained no indication that ERp57 (or PDI) associates with IP_3R1 (Supplemental Figure S6 online) or that ERp44 associates with SERCA 2b (data not shown).

Future Directions

To learn how ER lumenal conditions regulate the interaction between ERp44 and IP_3R1 and what the consequences of the interaction are in greater detail, it will be necessary to monitor ER lumenal conditions and the $[Ca^{2+}]_c$ in real time. It is also imperative to investigate the effect of ERp44 on IP_3R1 by using the planar lipid bilayer system under various conditions.

Finally, we were unable to find any protein in the brain (where IP_3R1 is exclusively expressed) that binds to the lumenal domain of IP_3R2 or IP_3R3, but these subtypes are likely to have different binding proteins that are not present in the brain. The fact that the cysteine residues in the L3V domain are conserved (Figure 1B) supports this hypothesis. Searching for such interacting protein(s), investigating how the lumenal environment regulates IP_3R2 and IP_3R3, and how it is related to ERp44/IP_3R1 are our next research challenges.

Experimental Procedures

Plasmids

Full-length ERp44 cDNA was obtained from P14 mouse cerebellum by the reverse transcriptase-polymerase chain reaction. The expression vectors for epitope-tagged or fluorescent protein-tagged ERp44, IP_3Rs, and their mutants were constructed by utilizing the polymerase chain reaction. The details of these methods, including the sequences of the primers used, will be supplied on request. All constructs were verified by DNA sequencing.

Antibodies

Rabbit polyclonal antibody to ERp44 was raised to purified His_6-ERp44 and affinity-purified with MBP-ERp44 coupled to CNBr-activated Sepharose 4B (Amersham). Other antibodies used were anti-IP_3R1 18A10, anti-IP_3R3 KM1082 (for both, see Hattori et al., 2004), anti-HA (12CA5, a gift of Dr. T. Yamamoto), anti-HA-Peroxidase (3F10, Roche), anti-CRT (Affinity BioReagents), anti-MBP (New England Biolabs), anti-human IgG (Vector Laboratories), anti-GST (Amersham), anti-GFP, and anti-actin (both Santa Cruz). The hybridoma producing anti-IgM (M-4 clone) was kindly provided by Dr. T. Kurosaki (Kansai Medical University).

Cell Culture and Transfection

COS-7, HeLa, and 293T cells were cultured in Dulbecco's modified Eagle medium supplemented with 10% heat-inactivated fetal bovine serum. DT40 cells were cultured in RPMI1640 medium supplemented with 10% heat-inactivated fetal bovine serum, 1% chicken serum, 100 U/ml penicillin and streptomycin, 2 mM glutamine, and 50 μM 2-mercaptoethanol. HeLa, COS-7, and 293T cells were transfected with expression vectors or siRNAs by means of TransIT (Mirus) or Lipofectamine2000 (Invitrogen). DT40 cells were transfected by electroporation with Nucleofector (Amaxa).

Identification of ERp44

1L3V-Fc or control Fc was expressed in 293T cells. After collecting the medium and incubating it with Protein-G Sepharose (Amersham) for 2 hr at 4°C, the beads were washed with 10 mM Tris-HCl (pH 8.0) and 150 mM NaCl. Approximately 0.2 mg of 1L3V-Fc or control Fc was coupled to beads, and the beads were loaded into a column. P14 mouse cerebella were washed with ice-cold PBS and homogenized in a buffer containing 0.32 M sucrose, 10 mM Tris-HCl (pH 7.5), 2 mM EDTA, and 1 mM DTT. The homogenates were centrifuged for 1 hr at 100,000 × *g* at 2°C, and after solubilizing the pellet in buffer containing 30 mM sodium acetate, 150 mM NaCl, 4 mM $CaCl_2$, and 1% Triton X-100, the solution was centrifuged at 10,000 × *g* for 15 min. The supernatant was applied to affinity columns, and the columns were washed with the same buffer, followed by neutral Ca^{2+} buffer (10 mM Tris-HCl [pH 8.0], 150 mM NaCl, 4 mM $CaCl_2$, and 1% Triton X-100), and finally neutral chelator buffer (10 mM Tris-HCl [pH 8.0], 150 mM NaCl, 5 mM EDTA, 5 mM EGTA, and 1% Triton X-100).

Western Blot Analysis

Proteins were resolved by SDS-PAGE and transferred to a polyvinylidene difluoride membrane. The membranes were blocked with 5% skim milk in PBS containing 0.05% Tween-20 (PBST) for 30 min and probed with the primary antibody for 3 hr at room temperature (RT). After washing with PBST, the membranes were incubated with a suitable secondary antibody and signals were detected with an ECL Plus kit (Amersham).

IP and GST-Pulldown Assay

For IP, cells were washed with PBS and then exposed to 2 mM DSP (Pierce) in PBS for 30 min at RT. After washing with PBS, the cells were solubilized in TNE buffer (150 mM Tris-HCl [pH 7.5], 500 mM NaCl, 1 mM EDTA, 1% Triton X-100, 0.1% SDS), and the lysates were incubated with the antibodies indicated and Protein-G Sepharose for 2 hr at 4°C. The beads were then washed five times with TNE buffer, and the proteins were eluted by boiling in SDS-PAGE sampling buffer.

Recombinant proteins were expressed in *E. coli* BL21 and purified with GSH-Sepharose (Amersham) or Amylose Resin (New England Biolabs). GST or GST fusion proteins were incubated with MBP or MBP fusion proteins for 1 hr at 4°C in acidic solution (30 mM NaOAc [pH 5.2], 150 mM NaCl, 4 mM $CaCl_2$, 0.1% Triton X-100). ERp44 and GST fusion proteins were incubated in neutral buffer (20 mM Tris-HCl [pH 7.5], 150 mM NaCl, 5 mM EGTA, 0.1% Triton X-100) with or without 3 mM DTT. GST-1L3V and MBP-ERp44 were incubated in neutral buffer or neutral buffer in which EGTA had been replaced with $CaCl_2$. The experiments in Figures 2D, 2E, 2J, and 2K were carried out in neutral buffer containing 3 mM DTT.

RNA Interference

SiRNA duplexes were purchased from Dharmacon. The target sequences were siControl-C (5'-AAGUAGUGUAUGCUAGAGUGG-3'), siERp44-C (5'-AAGUAGUGUUUGCCAGAGUUG-3'), siControl-3U (5'-AACAGCACCAUCGACCAACGU-3'), siERp44-3U (5'-AACAGCAGCAUCAACCUACGU-3').

Ca^{2+} Imaging

At 24–48 hr following transfection, cells were incubated for 30 min with 5 μM fura-2 AM (Dojindo). The cells were then placed on the stage of an inverted microscope (IX-70; Olympus, Japan) and perfused with balanced salt solution (BSS). Image capture and processing were performed with an Argus 50/CA system (Hamamatsu Photonics, Japan) at RT by a standard ratiometric method (excited at 340 nm and 380 nm). Fluorescence images of GFP and RFP were acquired separately and saved in the computer in the same optical fields as the fluorescence images for Ca^{2+} imaging. We also performed Ca^{2+}-imaging experiments using fura-4F AM in all cell types used in this study and confirmed that all of the responses obtained in experiments using fura-2 were not saturated (data not shown).

Planar Lipid Bilayer Experiments

Single-channel recordings of IP_3R1 in mouse cerebellar microsomes were performed as described previously (Michikawa et al., 1999), with some modifications. The *cis* chamber contained 108 mM Tris dissolved in 250 mM HEPES (pH 7.33), 1.11 mM K_2-H-HEDTA (N-hydroxyethylethylenediamine-N,N',N'-triacetic acid), 0.12 mM K-Ca-HEDTA. The *trans* chamber contained 250 mM HEPES (pH 7.33), 53 mM $Ba(OH)_2$, 3 mM DTT. IP_3R1 was activated by the addition of 6.4 μM IP_3 and 0.5 mM ATP to the *cis* chamber. Purified MBP or MBP-ERp44 was added directly to the *trans* side. The currents were amplified (Axon Instruments), filtered at 1 kHz with a low-pass Bessel filter (NF Instruments), and sampled at 10 kHz. Single-channel data were analyzed as described previously (Michikawa et al., 1999).

Acknowledgments

We thank K. Nakamura and A. Suzuki for excellent technical assistance and Dr. T. Inoue for invaluable discussions and technical help. We also thank Drs. A. Miyawaki, H. Bito, T. Shimizu, and A. Mizutani for critical reading of the manuscript. This study was supported by the grant from the JST, and the Grants-in-Aid (M.H. and K.M.) and The 21st Century COE Program, Center for Integrated Brain Medical Science, from the Ministry of Education, Culture, Sports, Science and Technology, Japan.

Received: April 28, 2004
Revised: August 24, 2004
Accepted: November 18, 2004
Published: January 13, 2005

References

Anelli, T., Alessio, M., Mezghrani, A., Simmen, T., Talamo, F., Bachi, A., and Sitia, R. (2002). ERp44, a novel endoplasmic reticulum folding assistant of the thioredoxin family. EMBO J. *21*, 835–844.

Anelli, T., Alessio, M., Bachi, A., Bergamelli, L., Bertoli, G., Camerini, S., Mezghrani, A., Ruffato, E., Simmen, T., and Sitia, R. (2003). Thiol-mediated protein retention in the endoplasmic reticulum: the role of ERp44. EMBO J. *22*, 5015–5022.

Bass, R., Ruddock, L.W., Klappa, P., and Freedman, R.B. (2003). A major fraction of ER-located glutathione is present as mixed disulfides with protein. J. Biol. Chem. *279*, 5257–5262.

Berridge, M.J. (2002). Neuronal calcium signaling. Neuron *21*, 13–26.

Berridge, M.J., Bootman, M.D., and Roderick, H.L. (2003). Calcium signalling: dynamics, homeostasis and remodelling. Nat. Rev. Mol. Cell Biol. *4*, 517–529.

Boehning, D., and Joseph, S.K. (2000). Functional properties of recombinant type I and type III inositol *1*, 4,5-trisphosphate receptor isoforms expressed in COS-7 cells. J. Biol. Chem. *275*, 21492–21499.

Camacho, P., and Lechleiter, J.D. (1995). Calreticulin inhibits repetitive intracellular Ca^{2+} waves. Cell *82*, 765–771.

Caroppo, R., Colella, M., Colasuonno, A., DeLuisi, A., Debellis, L., Curci, S., and Hofer, A.M. (2003). A reassessment of the effects of luminal $[Ca^{2+}]$ on inositol 1,4,5-trisphosphate-induced Ca^{2+} release from internal stores. J. Biol. Chem. *278*, 39503–39508.

Choe, C.U., Harrison, K.D., Grant, W., and Ehrlich, B.E. (2004). Functional coupling of chromogranin with inositol 1,4,5-trisphosphate receptor shapes calcium signaling. J. Biol. Chem. *279*, 35551–35556.

Foyouzi-Youssefi, R., Arnaudeau, S., Borner, C., Kelley, W.L., Tschopp, J., Lew, D.P., Demaurex, N., and Krause, K.H. (2000). Bcl-2 decreases the free Ca^{2+} concentration within the endoplasmic reticulum. Proc. Natl. Acad. Sci. USA *97*, 5723–5728.

Hattori, M., Suzuki, A.Z., Higo, T., Miyauchi, H., Michikawa, T., Nakamura, T., Inoue, T., and Mikoshiba, K. (2004). Distinct roles of inositol 1,4,5 trisphosphate receptor types 1 and 3. J. Biol. Chem. *279*, 11967–11975.

Hwang, C., Sinskey, A.J., and Lodish, H.F. (1992). Oxidized redox state of glutathione in the endoplasmic reticulum. Science *257*, 1496–1502.

Inoue, T., Kato, K., Kohda, K., and Mikoshiba, K. (1998). Type 1 inositol 1,4,5-trisphosphate receptor is required for induction of long-term depression in cerebellar Purkinje neurons. J. Neurosci. *18*, 5366–5373.

Kamp, F., Donoso, P., and Hidalgo, C. (1998). Changes in luminal pH caused by calcium release in sarcoplasmic reticulum vesicles. Biophys. J. *74*, 290–296.

Kim, J.H., Johannes, L., Goud, B., Antony, C., Lingwood, C.A., Daneman, R., and Grinstein, S. (1998). Noninvasive measurement of the pH of the endoplasmic reticulum at rest and during calcium release. Proc. Natl. Acad. Sci. USA *95*, 2997–3002.

Knapp, L.T., and Klann, E. (2002). Role of reactive oxygen species in hippocampal long-term potentiation: contributory or inhibitory? J. Neurosci. Res. *70*, 1–7.

Li, Y., and Camacho, P. (2004). Ca^{2+}-dependent redox modulation of SERCA 2b by ERp57. J. Cell Biol. *164*, 35–46.

Mattson, M.P. (2004). Pathways towards and away from Alzheimer's disease. Nature *430*, 631–639.

Meldolesi, J., and Pozzan, T. (1998). The endoplasmic reticulum Ca^{2+} store: a view from the lumen. Trends Biochem. Sci. *23*, 10–14.

Michikawa, T., Hirota, J., Kawano, S., Hiraoka, M., Yamada, M., Furuichi, T., and Mikoshiba, K. (1999). Calmodulin mediates calcium-dependent inactivation of the cerebellar type 1 inositol 1,4,5-trisphosphate receptor. Neuron *23*, 799–808.

Nishiyama, M., Hong, K., Mikoshiba, K., Poo, M.M., and Kato, K. (2000). Calcium stores regulate the polarity and input specificity of synaptic modification. Nature *408*, 584–588.

Orrenius, S., Zhivotovsky, B., and Nicotera, P. (2003). Regulation of cell death: the calcium-apoptosis link. Nat. Rev. Mol. Cell Biol. *4*, 552–565.

Paschen, W. (2003). Mechanisms of neuronal cell death: diverse roles of calcium in the various subcellular compartments. Cell Calcium *34*, 305–310.

Patterson, R.L., Boehning, D., and Snyder, S.H. (2004). Inositol 1,4,5-trisphosphate receptors as signal integrators. Annu. Rev. Biochem. *73*, 437–465.

Ro, H.A., and Carson, J.H. (2004). pH microdomains in oligodendrocytes. J. Biol. Chem. *279*, 37115–37123.

Roderick, L.H., Llewellyn, D.H., Campbell, A.K., and Kendall, J.M. (1998). Role of calreticulin in regulating intracellular Ca^{2+} storage and capacitative Ca^{2+} entry in HeLa cells. Cell Calcium *24*, 253–262.

Sevier, C.S., and Kaiser, C.A. (2002). Formation and transfer of disulphide bonds in living cells. Nat. Rev. Mol. Cell Biol. *3*, 836–847.

Stutzmann, G.E., Caccamo, A., LaFerla, F.M., and Parker, I. (2004). Dysregulated IP_3 signaling in cortical neurons of knock-in mice expressing an Alzheimer's-linked mutation in presenilin1 results in exaggerated Ca^{2+} signals and altered membrane excitability. J. Neurosci. *24*, 508–513.

Sugawara, H., Kurosaki, M., Takata, M., and Kurosaki, T. (1997). Genetic evidence for involvement of type 1, type 2 and type 3 inositol

1,4,5-trisphosphate receptors in signal transduction through the B-cell antigen receptor. EMBO J. *16*, 3078–3088.

Takei, K., Shin, R.M., Inoue, T., Kato, K., and Mikoshiba, K. (1998). Regulation of nerve growth mediated by inositol 1,4,5-trisphosphate receptors in growth cones. Science *282*, 1705–1708.

Tang, T.S., Tu, H., Chan, E.Y., Maximov, A., Wang, Z., Wellington, C.L., Hayden, M.R., and Bezprozvanny, I. (2003). Huntingtin and huntingtin-associated protein 1 influence neuronal calcium signaling mediated by inositol-(1,4,5) trisphosphate receptor type 1. Neuron *39*, 227–239.

Taylor, C.W., Genazzani, A.A., and Morris, S.A. (1999). Expression of inositol trisphosphate receptors. Cell Calcium *26*, 237–251.

Thrower, E.C., Choe, C.U., So, S.H., Jeon, S.H., Ehrlich, B.E., Yoo, S.H. (2003). A functional interaction between chromogranin B and the inositol 1,4,5-trisphosphate receptor/Ca^{2+} channel. J. Biol. Chem. *278*, 49699–49706.

Tu, B.P., and Weissman, J.S. (2002). The FAD- and O_2-dependent reaction cycle of Ero1-mediated oxidative protein folding in the endoplasmic reticulum. Mol. Cell *10*, 983–994.

Xiang, Y., Li, Y., Zhang, Z., Cui, K., Wang, S., Yuan, X.B., Wu, C.P., Poo, M.M., and Duan, S. (2002). Nerve growth cone guidance mediated by G protein-coupled receptors. Nat. Neurosci. *5*, 843–848.

The EMBO Journal (2004) 23, 1977–1986 | © 2004 European Molecular Biology Organization | All Rights Reserved 0261-4189/04
www.embojournal.org

THE EMBO JOURNAL

A novel protein-conjugating system for Ufm1, a ubiquitin-fold modifier

Masaaki Komatsu[1], Tomoki Chiba[1], Kanako Tatsumi[1], Shun-ichiro Iemura[2], Isei Tanida[3], Noriko Okazaki[4], Takashi Ueno[3], Eiki Kominami[3], Tohru Natsume[2] and Keiji Tanaka[1,*]

[1]Department of Molecular Oncology, Tokyo Metropolitan Institute of Medical Science, Bunkyo-ku, Tokyo, Japan, [2]National Institutes of Advanced Industrial Science and Technology, Biological Information Research Center (JBIRC), Kohtoh-ku, Tokyo, Japan, [3]Department of Biochemistry, Juntendo University School of Medicine, Bunkyo-ku, Tokyo, Japan and [4]Kazusa DNA Research Institute, Kazusa-Kamatari, Kisarazu, Chiba, Japan

Several studies have addressed the importance of various ubiquitin-like (UBL) post-translational modifiers. These UBLs are covalently linked to most, if not all, target protein(s) through an enzymatic cascade analogous to ubiquitylation, consisting of E1 (activating), E2 (conjugating), and E3 (ligating) enzymes. In this report, we describe the identification of a novel ubiquitin-fold modifier 1 (Ufm1) with a molecular mass of 9.1 kDa, displaying apparently similar tertiary structure, although lacking obvious sequence identity, to ubiquitin. Ufm1 is first cleaved at the C-terminus to expose its conserved Gly residue. This Gly residue is essential for its subsequent conjugating reactions. The C-terminally processed Ufm1 is activated by a novel E1-like enzyme, Uba5, by forming a high-energy thioester bond. Activated Ufm1 is then transferred to its cognate E2-like enzyme, Ufc1, in a similar thioester linkage. Ufm1 forms several complexes in HEK293 cells and mouse tissues, revealing that it conjugates to the target proteins. Ufm1, Uba5, and Ufc1 are all conserved in metazoa and plants but not in yeast, suggesting its potential roles in various multicellular organisms.
The EMBO Journal (2004) **23**, 1977–1986. doi:10.1038/sj.emboj.7600205; Published online 8 April 2004
Subject Categories: proteins
Keywords: Uba5; ubiquitin; ubiquitin fold; ubiquitin-like protein; Ufm1

Introduction

Protein modification plays a pivotal role in the regulation and expansion of genetic information. In the past two decades, a new type of post-translational protein-modifying system has been identified whose uniqueness is that protein(s) is used as a ligand, that is, modification of protein, by protein, and for protein. A typical system is the ubiquitylation, a modification system in which a single or multiple ubiquitin molecules are attached to a protein, which serves as a signaling player that controls a variety of cellular functions (Hershko and Ciechanover, 1998; Pickart, 2001). Protein ubiquitylation is catalyzed by an elaborate system highly regulated in the cells, which is catalyzed by a sequential reaction of multiple enzymes consisting of activating (E1), conjugating (E2), and ligating (E3) enzymes. E1, which initiates the reaction, forms a high-energy thiolester bond with ubiquitin via adenylation in an ATP-dependent manner. The E1-activated ubiquitin is then transferred to E2 in a thioester linkage. In some cases, E2 can directly transfer the ubiquitin to substrate proteins in an isopeptide linkage; however, E2s mostly requires the participation of E3 to achieve substrate-specific ubiquitylation reaction in the cells. E3s are defined as enzymes required for recognition of specific substrates for ubiquitylation, other than E1 and E2 (Varshavsky, 1997; Bonifacino and Weissman, 1998; Glickman and Ciechanover, 2002).

A set of novel molecules called ubiquitin-like proteins (UBLs) that have structural similarities to ubiquitin has been recently identified (Jentsch and Pyrowolakis, 2000). They are divided into two subclasses: type-1 UBLs, which ligate to target proteins in a manner similar, but not identical, to the ubiquitylation pathway, such as SUMO, NEDD8, and UCRP/ISG15, and type-2 UBLs (also called UDPs, ubiquitin-domain proteins), which contain ubiquitin-like structure embedded in a variety of different classes of large proteins with apparently distinct functions, such as Rad23, Elongin B, Scythe, Parkin, and HOIL-1 (Tanaka *et al*, 1998; Jentsch and Pyrowolakis, 2000; Yeh *et al*, 2000; Schwartz and Hochstrasser, 2003).

In this report, we describe a unique human UBL-type modifier named ubiquitin-fold modifier 1 (Ufm1) that is synthesized in a precursor form consisting of 85 amino-acid residues. We also identified the human activating (Uba5) and conjugating (Ufc1) enzymes for Ufm1. Prior to activation by Uba5, the extra two amino acids at the C-terminal region of the human proUfm1 protein are removed to expose Gly whose residue is necessary for conjugation to target molecule(s). Lastly, we show that the mature Ufm1 is conjugated to yet unidentified endogenous proteins, forming ~28, 38, 47, and 70 kDa complexes in human HEK293 cells and various mouse tissues.

Results

Identification of a novel protein-activating enzyme, Uba5

Our initial plan was to identify the molecule(s) that interacts with human Atg8p homolog GATE16, a type-1 UBL modifier required for autophagy (Klionsky and Emr, 2000; Ohsumi, 2001), using a yeast two-hybrid screening. Please note that the nomenclature of the autophagy-related genes was recently unified as *ATG* (Klionsky *et al*, 2003). Among several

*Corresponding author. Department of Molecular Oncology, The Tokyo Metropolitan Institute of Medical Science, 3-18-22 Honkomagome, Bunkyo-ku, Tokyo 113-8613, Japan. Tel.: +81 3 3823 2237; Fax: +81 3 3823 2237; E-mail: tanakak@rinshoken.or.jp

Received: 1 December 2003; accepted: 15 March 2004; published online: 8 April 2004

positive clones, we identified fragments of FLJ23251 (Figure 1A), which encodes a 404-amino-acid protein highly conserved in various multicellular organisms, such as *Homo sapiens*, *Caenorhabditis elegans*, *Drosophila melanogaster*, and *Arabidopsis thaliana*, but absent in yeasts (*Saccharomyces cerevisiae* and *Schizosaccharomyces pombe*) (Figure 1B). The sequence of FLJ23251 in the region containing residues 72–229 is highly homologous to the corresponding regions in Uba1 (i.e., E1 for ubiquitin) and other E1-like proteins for UBLs including the ATP-binding motif (GXGXXG) (Figure 1A and B). We named this protein Uba5, because it is a member of the E1-like enzyme family. Uba5 also has a metal-binding motif conserved in other E1-like enzymes such as Uba2, Uba3, Uba4, and Atg7. Most of E1-like enzymes have an active site Cys residue within the conserved 10–20 amino-acid residues downstream from the metal-binding

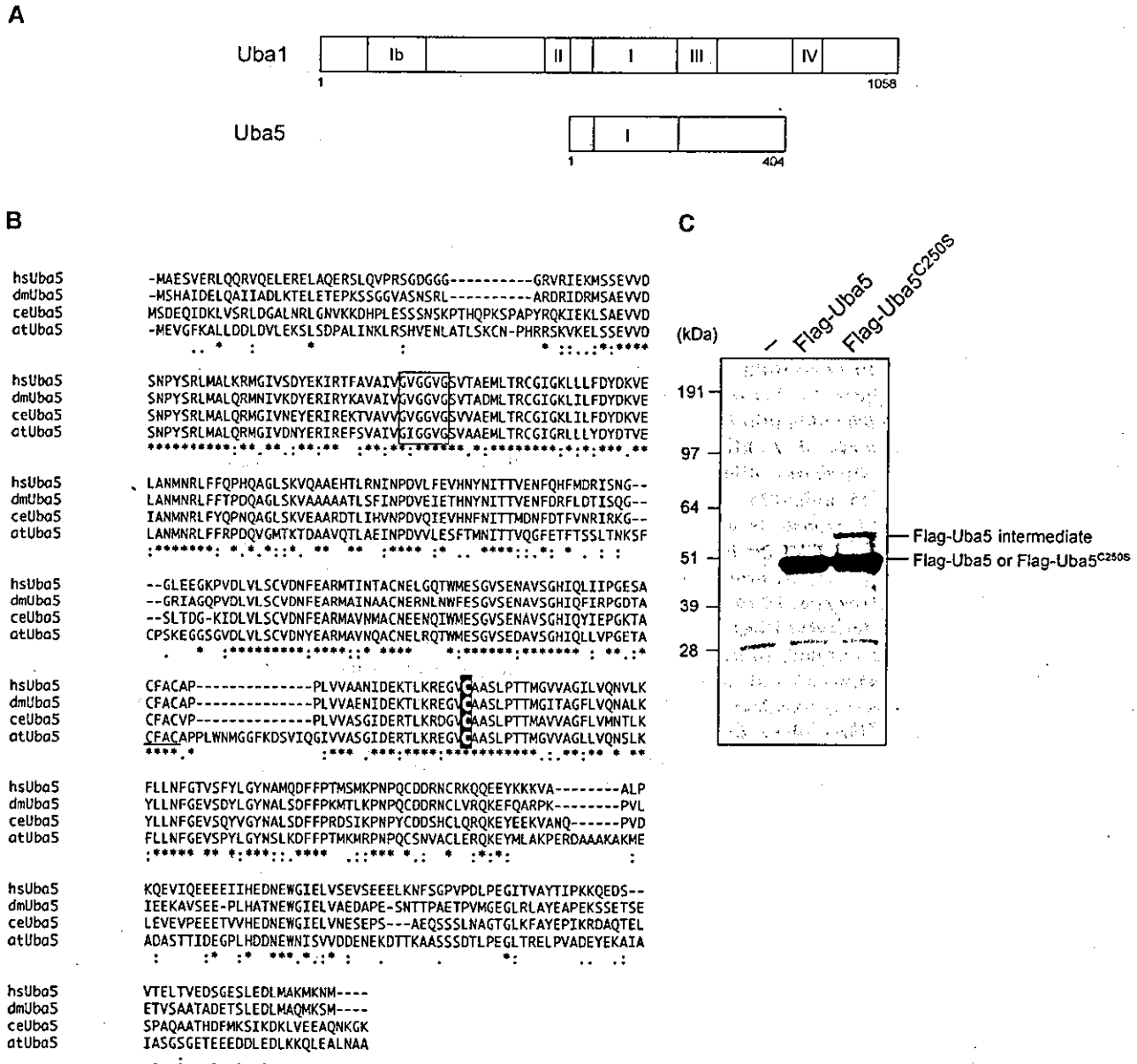

Figure 1 Uba5, a novel E1-like enzyme. (**A**) Schematic representation of Uba1 and Uba5 in *H. sapiens*. Uba1 is divided into several domains, including I, Ib, II, III, and IV boxes, which are conserved in other E1-like enzymes, and other regions without obvious similarity, described previously (Komatsu *et al*, 2001). Note that Uba5 is of a relatively small size and includes the box I and two other parts. The box I region of Uba1 (amino acids 459–611) has 48.4% similarity and 22.3% identity to amino acids 72–229 of Uba5, which includes the conserved ATP-binding motif (GXGXXG). The sequence of Uba5 is available from GenBank^{TM} under the accession number AK026904. hs, *H. sapiens*; ce, *C. elegans*; dm, *D. melanogaster*; at, *A. thaliana*. (**B**) Sequence alignment of hsUba5 and its homologs of other species (dm, NM_132494; ce, NM_058847; at, NM_100414). The amino-acid sequence of hsUba5 is compared by the ClustalW program. *Asterisks*, identical amino acids; *single* and *double dots*, weakly and strongly similar amino acids, respectively, determined by the criteria of ClustalW program. *Open box* indicates an ATP-binding motif. The putative active site Cys residue is boxed in black. The metal-binding motif is underlined. (**C**) Identification of the intermediate linked to Uba5 in HEK293 cells. Both Uba5 and Uba5^{C250S}, in which the predicted active site Cys positioned at 250 was changed to Ser by site-directed mutagenesis, were tagged with Flag peptide at N-terminus, resulting in Flag-Uba5 and Flag-Uba5^{C250S}, respectively. Each Flag-Uba5 and Flag-Uba5^{C250S} was expressed in HEK293 cells. The cell lysates were subjected to SDS-PAGE and analyzed by immunoblotting with anti-Flag antibody.

motif. In the case of Uba5, the Cys^{250} seems to be the most possible active site Cys residue (Figure 1B). If an active site Cys residue within an E1 and E1-like enzymes is changed to Ser, an O-ester bond instead of a thioester bond is formed with its respective modifier protein and the intermediates become stable even under reducing conditions. Therefore, we mutated Cys^{250} within Uba5 to Ser and expressed it as a Flag-fused $Uba5^{C250S}$ (Flag-$Uba5^{C250S}$) or Flag-Uba5 as control in HEK293 cells. As shown in Figure 1C, both Flag-Uba5 and Flag-$Uba5^{C250S}$ were expressed as ~50 kDa proteins in HEK293 cells. When Flag-$Uba5^{C250S}$ was expressed, an additional band with a higher molecular mass of ~60 kDa was clearly observed, indicating that Flag-$Uba5^{C250S}$ forms an intermediate complex with an endogenous protein. These results suggest that Uba5 is indeed a novel protein-activating enzyme for a presumptive modifier (see below).

Identification of a novel ubiquitin-fold molecule, Ufm1

Because Uba5 was identified as GATE-16-binding protein, we initially assumed that Uba5 is another GATE-16-activating enzyme, in addition to Atg7. To test this possibility, we examined whether $Uba5^{C250S}$ (the presumptive active site Cys at position 250 was replaced by Ser) forms an intermediate complex with GATE-16 or not. Unexpectedly, we could not identify a stable complex between $Uba5^{C250S}$ and GATE-16 (data not shown). Therefore, we attempted to identify a protein(s) that physically associates with Uba5 in the cells. To do this, Flag-Uba5 was expressed in HEK293 cells, then immunoprecipitated by anti-Flag antibody. The immunoprecipitates were eluted with a Flag peptide, then digested with Lys-C endopeptides (*Achromobacter* protease I) and the cleaved fragments were directly analyzed using a highly sensitive 'direct nano-flow LC–MS/MS' system as described in Materials and methods. Following database search, a total of 28 peptides were assigned to MS/MS spectra obtained from four nano-LC–MS/MS analyses for the Flag-Uba5-associated complexes. These peptide data identified three proteins as Uba5-associated components: GATE-16, and hypothetical proteins BM-002 and CGI-126 (excluding the bait protein Uba5 and the background proteins, such as HSP70 and keratins).

One of these identified proteins, BM-002, is an 85-amino-acid protein with a predicted molecular mass of ~9.1 kDa. This protein is conserved in multicellular organisms, but not in yeasts, like Uba5 (Figure 2A). The human BM-002 has high identity over the species in the central region but has elongated sequences at both N- and C-terminal regions in some species. Although the protein shows no clear overall sequence identity to ubiquitin or other modifiers (Figure 2B), the tertiary structure of BM-002 displays a striking resemblance to human ubiquitin (Figure 2C). The human structure of BM-002 was constructed by a computer-assisted modeling, based on the structure of its *C. elegans* homolog that has been analyzed previously, as a protein possessing 'ubiquitin-like fold' with secondary structure elements ordered β–β–α–β–β–α (α-helix and β-sheet) along the sequence (Cort *et al*, 2002). Thus, we named human BM-002 as Ufm1.

Ubiquitin is synthesized in a precursor form that must be processed by de-ubiquitylating enzymes (DUBs) to generate a Gly–Gly sequence at the C-terminus. Similarly, Ufm1 has a single Gly residue conserved across species at the C-terminal region, although the length and sequences of amino acids extending from this Gly residue vary among species. To test whether the C-terminus of Ufm1 is post-translationally cleaved, we constructed an expression vector for Ufm1 tagged at both the N- and C-ends, that is, a Flag epitope at the N-terminus and an HA epitope at the C-terminus (Flag-Ufm1-HA) (Figure 2D). After transfection of Flag-Ufm1-HA into HEK293 cells, the cell lysate was subjected to SDS–PAGE, and Flag-Ufm1-HA was detected by immunoblotting. A 10-kDa protein corresponding to Ufm1 was recognized with anti-Flag antibody, while no appreciable protein was observed with anti-HA antibody (Figure 2E, lanes 2 and 7). The mobility on SDS–PAGE was similar to that of Flag-Ufm1ΔC2 (equivalent to mature $Ufm1^{1-83}$ protein) lacking the C-terminal Ser^{84} and Cys^{85} of proUfm1 (Figure 2E, lane 4). These results suggested that the C-terminus of Ufm1 is post-translationally cleaved in the cells, producing mature Ufm1 with the C-terminal Gly^{83} residue. It is known that the replacement of C-terminal Gly residue of Ub and other UBLs with an Ala residue inhibits the C-terminal processing (Kabeya *et al*, 2000; Tanida *et al*, 2003). To examine whether Gly^{83} of Ufm1 is essential for the cleavage, Gly^{83} of Flag-Ufm1-HA was mutated to Ala, and expressed in HEK293 cells (Figure 2D, Flag-$Ufm1^{G83A}$-HA). The mobility of most Flag-$Ufm1^{G83A}$-HA on SDS–PAGE was apparently slower than that of Flag-Ufm1-HA (Figure 2E, lane 3). This mutant was recognized by immunoblotting with anti-HA antibody as well as anti-Flag antibody, suggesting that mutation Gly^{83} to Ala confers resistance to its C-terminal cleavage.

Uba5 is an Ufm1-activating enzyme

We next investigated whether Uba5 forms an intermediate complex with Ufm1. We expressed Flag-Uba5 or Flag-$Uba5^{C250S}$ with Myc-tagged Ufm1 (Myc-Ufm1) in HEK293 cells. Myc-tagged Ufm1ΔC3 lacking the C-terminal Gly^{83} of mature Ufm1 (Myc-Ufm1ΔC3; i.e., deletion form of three residues from precursor $Ufm1^{1-85}$ protein) was used as control. Each cell lysate was prepared and analyzed by immunoblotting with anti-Flag antibody. Flag-$Uba5^{C250S}$ formed an intermediate with an endogenous protein as shown in Figure 1 (Figure 3A, lane 7). When Flag-$Uba5^{C250S}$ was coexpressed with Myc-Ufm1, the intermediate shifted to higher molecular weight (Figure 3A, lane 8). The higher band was not detected when Myc-Ufm1ΔC3 was coexpressed (Figure 3A, lane 9). To verify that the intermediate is indeed the Uba5–Ufm1 complex, Flag-$Uba5^{C250S}$ was immunoprecipitated and blotted with anti-Flag and anti-Myc antibody. Consistent with the above data, a higher sized intermediate was observed when Flag-$Uba5^{C250S}$ was coexpressed with Myc-Ufm1 (Figure 3B, top panel, lane 5), but not alone or with Myc-Ufm1ΔC3 (Figure 3B, top panel, lanes 4 and 6). The intermediate was also recognized by anti-Myc antibody (Figure 3B, lower panel, lane 5), indicating the existence of the Flag-$Uba5^{C250S}$–Myc-Ufm1 complex. Note that the small-sized intermediate is presumably a complex with an endogenous Ufm1, as mentioned. These results indicate that Uba5 forms an intermediate with Ufm1 and the Gly^{83} residue of Ufm1 is essential for the formation of the intermediate with Uba5 *in vivo*.

We subsequently tested whether Uba5 can activate Ufm1 *in vitro*. The thioester formation assay was performed using recombinant proteins expressed in *Escherichia coli*. Recombinant GST-tagged Uba5 and mature Ufm1

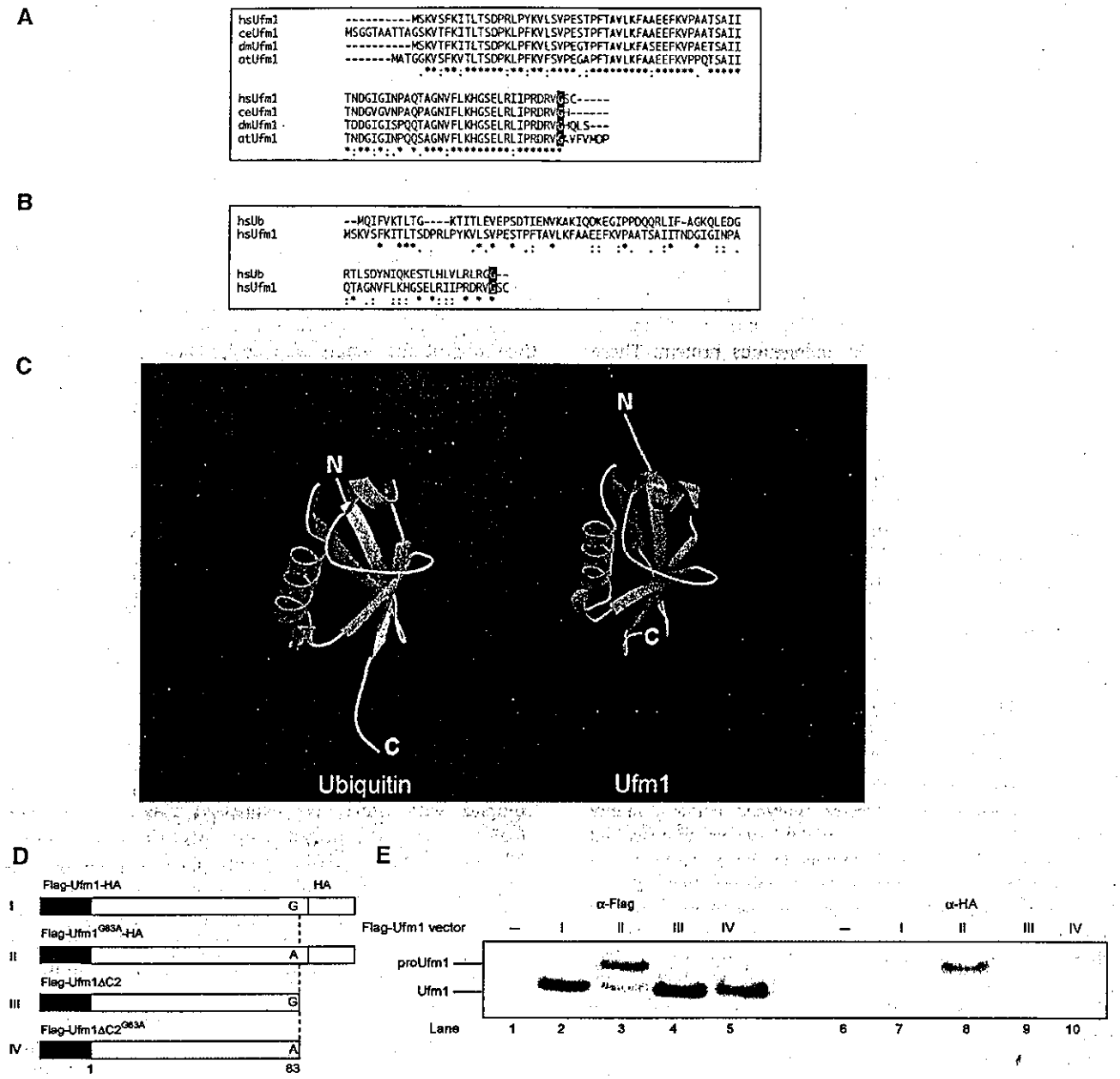

Figure 2 Ufm1, a novel ubiquitin-fold molecule. (**A**) Sequence alignment of hsUfm1 and its homologs. The sequence of hsUfm1 is available from GenBank™ under the accession number BC005193 (dm, a coding region of dmUfm1 was found from *D. melanogaster* genomic sequence; ce, NM_066304; at, NM_106420). The homology analysis was performed as described in Figure 1B. The C-terminal conserved Gly residue is boxed in black. (**B**) Sequence alignment of hsUbiquitin with hsUfm1. The homology analysis was performed as described in Figure 1B. The C-terminal conserved Gly residue is boxed in black. (**C**) Structural ribbon of hsUbiquitin and predicted structural ribbon of hsUfm1. α-Helices and β-strands are shown in green and yellow, respectively. The homology model of hsUfm1 was created from the *C. elegans* Ufm1 structure (Cort *et al*, 2002) by using MOE program (2003.02; Chemical Computing Group Inc., Montreal, Quebec, Canada). (**D**) Schematic representation of mammalian expression plasmids for Ufm1 and the derivative mutants. Flag epitope tags at the N-terminus, HA epitope tags at the C-terminus, and putative cleavage site Gly^{83} residue (vertical dotted lines) are indicated. To construct $Ufm1^{G83A}$, a single point mutation was introduced into Ufm1, which led to an amino-acid substitution from Gly to Ala at position 83. To construct Ufm1ΔC2, the two C-terminal residues were deleted by PCR. $Ufm1\Delta C2^{G83A}$ was also produced by site-directed mutagenesis of Ufm1ΔC2. The ΔC2 mutants were tagged with the Flag epitopes at N-terminus. (**E**) ProUfm1 processing. HEK293 cells were transfected with Flag-Ufm1-HA, Flag-$Ufm1^{G83A}$-HA, Flag-Ufm1ΔC2, or Flag-$Ufm1\Delta C2^{G83A}$. The cell lysates were subjected to SDS–PAGE and analyzed by immunoblots with anti-Flag and anti-HA antibodies. ProUfm1 and mature Ufm1 are indicated on the left. The numbers at the top from I to IV are similar to those in (D).

(Ufm1ΔC2) with exposed C-terminal Gly^{83} residue were purified, mixed and incubated in the presence of ATP and then subjected to SDS–PAGE at either reducing or nonreducing conditions. GST-Ufm1ΔC3 was used as control. An ~100 kDa band corresponding to the GST-Ufm1ΔC2–GST-Uba5 intermediate complex was clearly observed when the mixture was applied at nonreducing conditions (Figure 3C, lane 3). This intermediate was not observed when ATP or GST-Uba5 was excluded from the mixture (Figure 3C, lanes 1 and 2), or when the mixture was loaded in the presence of

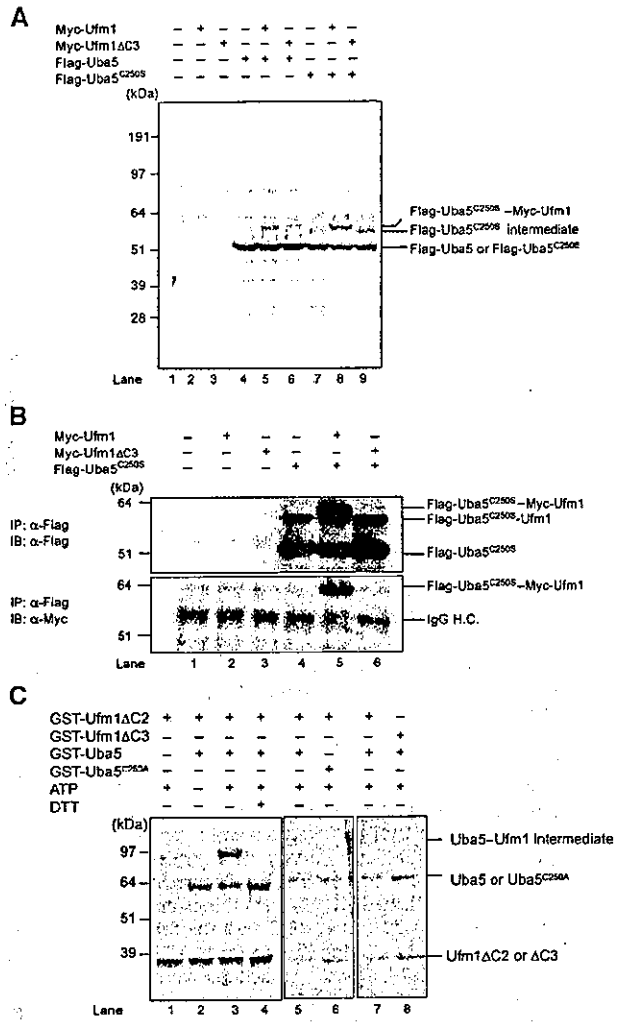

Figure 3 Demonstration that Uba5 is an Ufm1-activating enzyme. (A) Immunoblotting analysis. Each Myc-tagged Ufm1 (Myc-Ufm1) and Myc-Ufm1ΔC3 was expressed alone (lanes 2 and 3, respectively), and coexpressed with Flag-Uba5 (lanes 5 and 6, respectively) or Flag-Uba5^{C250S} (lanes 8 and 9, respectively). Each Flag-Uba5 and Flag-Uba5^{C250S} was also expressed alone (lanes 4 and 7, respectively). The cell lysates were subjected to SDS–PAGE and analyzed by immunoblotting with anti-Flag antibody. The bands corresponding to Flag-Uba5, Flag-Uba5^{C250S}, and Flag-Uba5^{C250S} intermediates are indicated on the right. (B) Immunoblotting analysis after immunoprecipitation. Each Myc-Ufm1 and Myc-Ufm1ΔC3 was expressed alone (lanes 2 and 3, respectively), and coexpressed with Flag-Uba5^{C250S} (lanes 5 and 6, respectively). Flag-Uba5^{C250S} was also expressed alone (lane 4). The cell lysates were immunoprecipitated with anti-Flag antibody. The resulting immunoprecipitates were subjected to SDS-PAGE and analyzed by immunoblotting with anti-Flag and anti-Myc antibodies. The bands corresponding to Flag-Uba5^{C250S}, Flag-Uba5^{C250S}–endogenous Ufm1, and Flag-Uba5^{C250S}–Myc-Ufm1 intermediates are indicated. (C) *In vitro* activating assay of Ufm1 by Uba5. Purified recombinant GST-Ufm1ΔC2 (2 μg) (lanes 1–7) was incubated for 30 min at 25°C with some of the following: 2 μg of purified recombinant GST-Uba5 (lanes 2–5, 7, and 8), GST-Uba5^{C250A} (lane 6), and 5 mM ATP (lanes 1 and 3–8). Lane 8 was conducted similar to lane 7, except that GST-Ufm1ΔC3 was used instead of GST-Ufm1ΔC2. Reactions were then incubated with SDS loading buffer lacking reducing agent (lanes 1–3 and 5–8) or containing 100 mM DTT (lane 4). The presence or absence of various components is indicated above the lanes. The bands corresponding to free GST-Uba5, GST-Uba5^{C250A}, GST-Ufm1ΔC2 (mature Ufm1), GST-Ufm1ΔC3, and GST-Uba5–GST-Ufm1ΔC2 thioester product are indicated on the right.

a reducing agent dithiothreitol (DTT) (Figure 3C, lane 4). Furthermore, GST-tagged Uba5^{C250A} mutant, a presumptive active site Cys mutant, could not form the intermediate even at nonreducing conditions (Figure 3C, lane 6). GST-tagged Ufm1ΔC3 was also incapable of forming the intermediate in this reaction (Figure 3C, lane 8). Taken together, we concluded that Uba5 is an Ufm1-activating enzyme and has the active site in Cys^{250}.

Identification of a novel protein-conjugating enzyme, Ufc1

The LC–MS/MS analysis revealed CGI-126 protein as another Uba5 interacting protein. CGI-126 is a protein of 167-amino-acid residues with a predicted molecular mass of 19.4 kDa. This protein is also conserved in multicellular organisms, like Uba5 and Ufm1 (Figure 4A). The C-terminal half of human CGI-126 has a high identity across species as shown in Figure 4A. CGI-126 has a highly conserved region, for example, residues 113–126, with limited similarity to the region of Ubc's that encodes an active site Cys residue capable of forming a thioester bond (Figure 4A). We assumed that this protein may be an E2-like conjugating enzyme for Ufm1 and thus named it Ufm1-conjugating enzyme 1 (Ufc1). If Ufc1 is an authentic E2 enzyme for Ufm1, it is expected to form an intermediate complex with Ufm1 via a thioester linkage. To test this possibility in the same way as Uba5, we mutated the predicted active site Cys residue within Ufc1 (Figure 4A, Cys^{116}) to Ser. We expressed Flag-Ufc1 or Flag-Ufc1^{C116S} (a presumptive active site Cys at position 116 was replaced by Ser) in combination with Myc-Ufm1 or Myc-Ufm1ΔC3 in HEK293 cells. Flag-Ufc1^{C116S} formed a stable intermediate band when coexpressed with Myc-Ufm1 (Figure 4B, lane 8), but not alone or with Myc-Ufm1ΔC3 (Figure 4B, lanes 7 and 9). To ascertain that this is the Flag-Ufc1^{C116S}–Myc-Ufm1 intermediate, Flag-Ufc1^{C116S} was immunoprecipitated and blotted with anti-Myc antibody (Figure 4C). Indeed, Myc-Ufm1, but not Myc-Ufm1ΔC3, formed a complex with Flag-Ufc1^{C116S} (Figure 4C, lanes 5 and 6, top and bottom panels). Note that Flag-Ufc1^{C116S} intermediate with a faster electrophoretic mobility than the Flag-Ufc1^{C116S}–Myc-Ufm1 complex is presumably the intermediate with the endogenous Ufm1 (Figure 4C, lanes 4–6, upper panel). These results indicate that Ufc1 forms an intermediate with Ufm1 *in vivo*.

To confirm that Ufc1 is indeed an E2-like enzyme that conjugates with Ufm1 *via* a thioester linkage, we conducted an *in vitro* Ufm1 conjugation assay. Recombinant GST-Uba5, GST-Ufc1, and GST-Ufm1ΔC2 were mixed and incubated in the presence of ATP. GST-Ufc1^{C116A} mutant and GST-Ufm1ΔC3 were used as negative controls. Under nonreducing conditions, an ~70 kDa band corresponding to GST-Ufm1ΔC2–GST-Ufc1 intermediate was observed (Figure 4D, lane 4). This product was not formed at reducing conditions, or when any of the components was omitted from the reaction (Figure 4D, lanes 1–3 and 5). GST-tagged Ufc1^{C116A} mutant could not form the intermediate, suggesting that Cys116 is indeed the active site (Figure 4D, lane 7). GST-Ufm1ΔC3 was again unable to form the intermediate complex in this reaction (Figure 4D, lane 9). Taken together, we concluded that Ufc1 functions as an Ufm1-conjugating enzyme and has the active site in Cys^{116}.

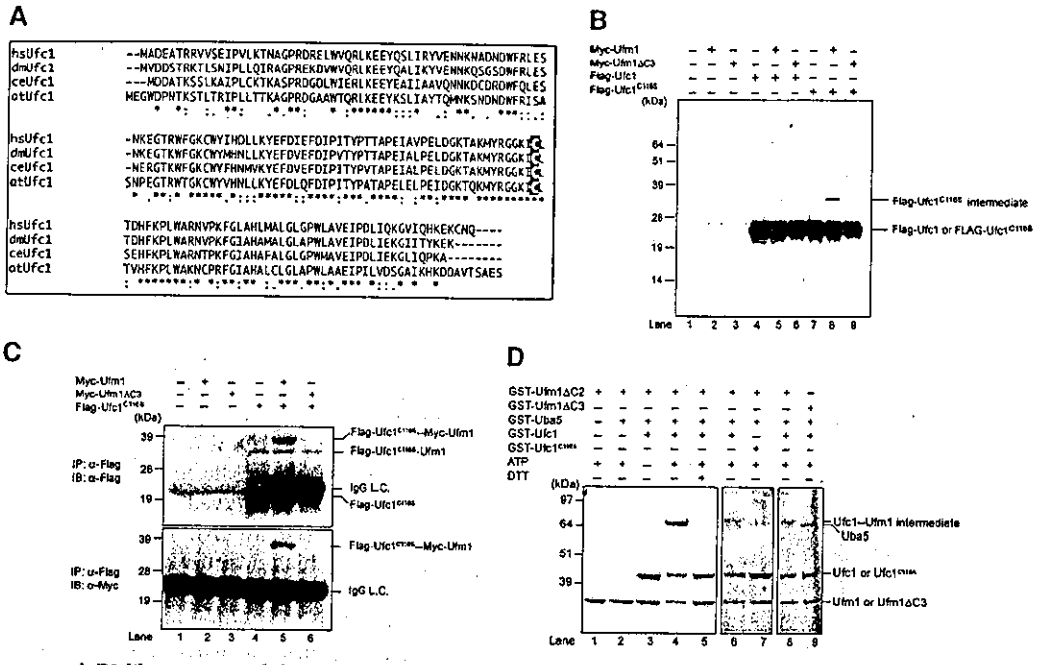

Figure 4 Ufc1, a novel E2-like enzyme. (**A**) Sequence alignment of hsUfc1 and its homologs. The sequence of Ufc1 is available from GenBank™ under the accession number BC005187 (dm, NM_137230; ce, NM_066654; at, BT001180). The homology analysis was performed as described in Figure 1B. The putative active site Cys residue is boxed in black. (**B**) Immunoblotting analysis. Each Myc-tagged Ufm1 (Myc-Ufm1) and Myc-Ufm1ΔC3 was expressed alone (lanes 2 and 3, respectively), and coexpressed with Flag-Ufc1 (lanes 5 and 6, respectively) or Flag-Ufc1^{C116S} (lanes 8 and 9, respectively). Each Flag-Ufc1 and Flag-Ufc1^{C116S} was also expressed alone (lanes 4 and 7, respectively). The cell lysates were subjected to SDS–PAGE and analyzed by immunoblotting with anti-Flag antibody. The bands corresponding to Flag-Ufc1, Flag-Ufc1^{C116S}, and Flag-Ufc1^{C116S} intermediates are indicated on the right. (**C**) Immunoblotting analysis after immunoprecipitation. Each Myc-Ufm1 and Myc-Ufm1ΔC3 was expressed alone (lanes 2 and 3, respectively), and coexpressed with Flag-Ufc1^{C116S} (lanes 5 and 6, respectively). Flag-Ufc1^{C116S} was also expressed alone (lane 4). The cell lysates were immunoprecipitated with anti-Flag antibody. The resulting immunoprecipitates were subjected to SDS–PAGE and analyzed by immunoblots with anti-Flag and anti-Myc antibodies. The bands corresponding to Flag-Ufc1^{C116S}, Flag-Ufc1^{C116S}–endogenous Ufm1, and Flag-Ufc1^{C116S}–Myc-Ufm1 intermediates are indicated. (**D**) *In vitro* thioester bond formation assay of Ufm1 by Ufc1. Purified recombinant GST-Ufm1ΔC2 (2 μg) (lanes 1–8) was incubated for 30 min at 25°C with the following: purified recombinant GST-Uba5 (0.2 μg) (lanes 2–9), GST-Ufc1 (2 μg) (lanes 3–6, 8, and 9), GST-Ufc1^{C116S} (2 μg) (lane 7), and 5 mM ATP (lanes 1, 2, and 4–9). Lane 9 was conducted similar to lane 8, except that GST-Ufm1ΔC3 was used instead of GST-Ufm1ΔC2. Reactions were then incubated with SDS loading buffer lacking reducing agent (lanes 1–4 and 6–9) or containing 100 mM DTT (lane 5). The presence or absence of various components is indicated above the lanes. The bands corresponding to free GST-Ufm1ΔC2 (mature Ufm1), GST-Ufm1ΔC3, GST-Uba5, GST-Ufc1, GST-Ufc1^{C116S}, and GST-Ufc1–GST-Ufm1ΔC2 thioester product are indicated on the right.

Conjugation of Ufm1 to cellular protein(s)

We next examined whether Ufm1 conjugates to the target protein(s) in cells. To this end, we expressed Flag- and 6xHis-tagged Ufm1 constructs in HEK293 cells, and purified them under denaturing conditions by Ni^{2+} beads. The resulting precipitates were then analyzed by immunoblotting with anti-Flag antibody. When FlagHis-Ufm1-HA (proUfm1) or FlagHis-Ufm1ΔC2 (mature form) was expressed, several proteins with sizes of about 28, 38, and 47 kDa were detected, in addition to the 10 kDa corresponding to free FlagHis-Ufm1ΔC2 (Figure 5A, lanes 2 and 4). These bands were not detected by FlagHis-Ufm1^{G83A}-HA and FlagHis-Ufm1ΔC3, suggesting that both C-terminal cleavage and C-terminal Gly residue are required for the conjugation reaction (Figure 5A, lanes 3 and 6). Moreover, these protein bands were resistant to reducing agents, such as DTT and β-mercaptoethanol. These results indicate that Ufm1 is covalently attached to some target proteins, probably through an isopeptide bond between the C-terminal Gly^{83} of Ufm1 and a Lys residue in the cellular proteins. It is of note that FlagHis-Ufm1^{G83A} mutant with exposed C-terminal Ala instead of Gly can conjugate to target proteins (Figure 5A, lane 5), consistent with the previous report on ubiquitin and SUMO (Hodgins *et al*, 1992; Kamitani *et al*, 1997). Since C-terminal Gly to Ala mutation confers resistance to the Ufm1 processing, the conjugates with FlagHis-Ufm1^{G83A} mutant may be more stable than those with FlagHis-Ufm1ΔC2 (Figure 5A, compare lanes 4 and 5). These results suggest that the Ufm1 conjugation is also a reversible reaction.

We further investigated the expression of Ufm1 and its conjugated proteins in mouse tissues using anti-Ufm1 serum. Ufm1 was widely expressed in all tissues examined, such as brain, heart, lung, liver, and kidney (Figure 5B, left panel). In addition, several bands with striking similarity to proteins detected in HEK293 cells were observed. These bands were not detected by preimmune or preabsorbed antisera (Figure 5B, right panel), suggesting that they are likely the Ufm1 conjugates. Although the intensity of each band varied among tissues and HEK293 cells, 28 and 38 kDa proteins were commonly detected. The 70-kDa band observed in all tissues was also detected faintly in HEK293 cells (Figure 5A, lane 5). The 47-kDa band observed in HEK293 cells was not clear. These protein bands were resistant to reducing agents, such as DTT and β-mercaptoethanol, indicating that Ufm1 covalently attaches to cellular proteins like other Ubl proteins. The targets of Ufm1 appeared to be common in a variety

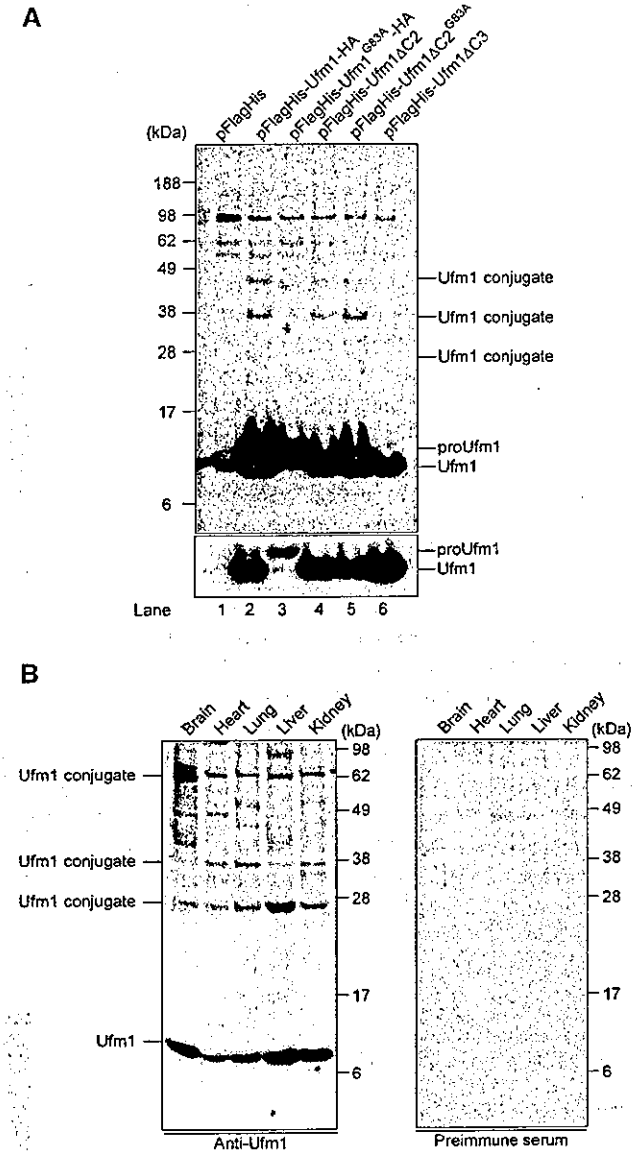

Figure 5 Formation of a covalent protein conjugate(s) with Ufm1 in HEK293 cells and mouse tissues. (**A**) Ufm1 conjugates in human HEK293 cells. HEK293 cells were transfected with FlagHis-Ufm1-HA, FlagHis-Ufm1^{G83A}-HA, FlagHis-Ufm1ΔC2, FlagHis-Ufm1ΔC2^{G83A}, or FlagHis-Ufm1ΔC3 expression plasmids. These cells were lysed under denaturing conditions, and the lysates were precipitated with Ni^{2+} beads. The precipitates were subjected to SDS–PAGE and analyzed by immunoblotting with anti-Flag antibody. The bottom panel shows the short exposure of the upper panel. The bands corresponding to mature Ufm1, proUfm, and Ufm1 conjugates are indicated on the right. (**B**) Ufm1 conjugates in various mouse tissues. Homogenates from mouse tissues as indicated were prepared and subjected to SDS–PAGE and analyzed by immunoblotting with anti-Ufm1 serum (left panel) or preimmune serum (right panel). The bands corresponding to Ufm1 and conjugates between Ufm1 and target proteins are indicated on the left.

of tissues. These results suggest the universal roles of Ufm1 in the regulation of cellular function in multicellular organisms.

Subcellular localization of Ufm1 in HeLa cells

We finally examined the subcellular distribution of Ufm1 in HeLa cells. Immunocytochemical analysis using anti-Ufm1

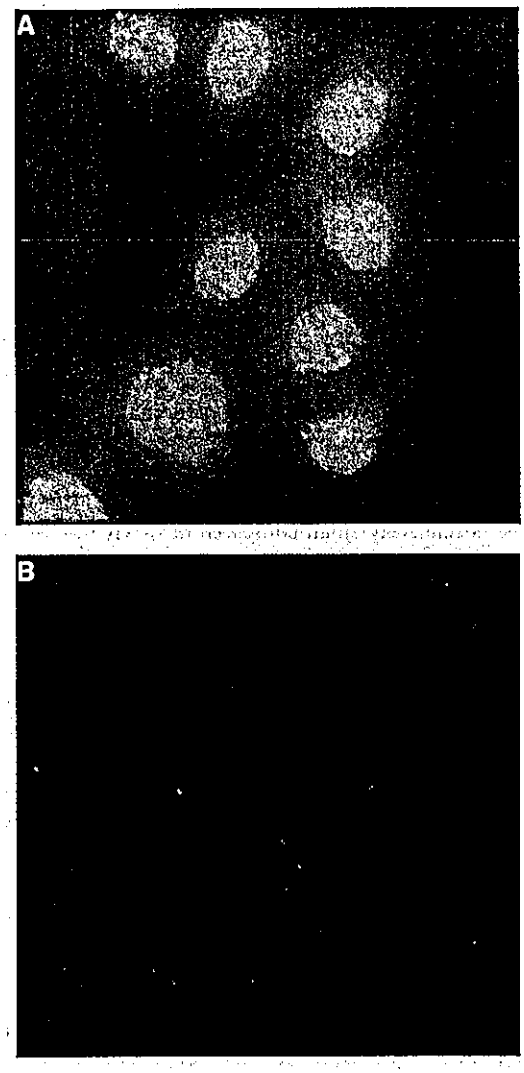

Figure 6 Intracellular distribution of Ufm1 in HeLa cells. (**A**) HeLa cells were seeded on coverslips 24 h before fixation for immunostaining. Ufm1 was detected with anti-Ufm1 serum and visualized with Alexa 488 nm anti-rabbit antibody. (**B**) Immunocytochemical analysis was conducted as for (A), except that preimmune serum was used. Cells were observed using a fluorescence microscope. Magnification, × 400.

serum revealed that Ufm1 was predominantly localized in the nucleus and diffusely in the cytoplasm (Figure 6A). These staining patterns were not observed when anti-Ufm1 serum had been preadsorbed with excess amounts of recombinant Ufm1 protein or preimmune serum was used instead of anti-Ufm1 serum (Figure 6B). Moreover, Ufm1 localization in the cytoplasm and nucleus was similar to the localization of exogenously expressed GFP-tagged Ufm1 in HeLa cells (data not shown). In the nucleus, strong immunoreactivity to anti-Ufm1 serum was observed as a dot-like structure. Although such dots-like structures were detected by preimmune serum, those intensities were weak. Thus, some of these dot-like structures may represent conjugates of Ufm1.

Discussion

In the present study, we reported that Ufm1 acts as a new post-translational UBL modifier, based on the following

criteria: (1) It is a small protein of 9.1 kDa with a ubiquitin-fold structure. (2) Ufm1 is synthesized in a precursor form, and the extra amino-acid residues at the C-terminal side need to be processed to expose the Gly residue. (3) The C-terminal processing and exposure of glycine residue are essential to the formation of Ufm conjugates in the cells. (4) Ufm1 has specific E1-like (Uba5) and E2-like (Ufc1) enzymes for activation and conjugation, respectively. Intriguingly, many UBL modifiers are evolutionarily conserved from yeast to human, except interferon-inducible UBL modifiers, such as UCRP/ISG15, Fat10, and Fau1/MNSFβ (Nakamura *et al*, 1995; D'Cunha *et al*, 1996; Liu *et al*, 1999). Ufm1, Uba5, and Ufc1 found in the present study are conserved in various multicellular organisms (Figures 1B, 2A, and 4A), but not in both budding and fission yeasts, suggesting that they all have been generated by coevolution.

We identified Uba5 as an E1 enzyme for Ufm1. This enzyme is relatively small compared to Uba1, that is, an E1 for ubiquitin (Figure 1A). In the *in vitro* assay, the recombinant Uba5 protein formed a thioester linkage with recombinant Ufm1 (Figure 3C) and transferred the activated Ufm1 to recombinant Ufc1 (an E2 enzyme) (Figure 4D), indicating that Uba5 can activate Ufm1 as a single molecule. This is in marked contrast to other E1s such as Uba2 and Uba3, which retain obvious similarities to the C-terminal half of Uba1 but require the formation of heterodimer complexes with respective partner molecules, AOS1 and APP-BP1, respectively, with similarities to the N-terminal half of Uba1 (Johnson *et al*, 1997; Liakopoulos *et al*, 1998; Osaka *et al*, 1998). Another E1-like enzyme, Uba4 that activates Urm1, is of similar size to Uba5 (Furukawa *et al*, 2000), but it remains unknown whether Uba4 acts as a single molecule or needs a partner subunit. The homology of Uba5 to Uba1 is less than those of Uba2 and Uba3, except their ThiF domain conserved in E1s, and thus it is likely that Uba5 may uniquely activate Ufm1, differing from other E1s such as Uba1, Uba2/AOS1, and Uba3/APP-BP1. Thus, although the structure of APP-BP1/Uba3 heterodimer is determined and the mechanism by which E1s activate their cognate UBLs was proposed (Walden *et al*, 2003a, b), the weak homology of Uba5 with other E1s hampered the computer-assisted structural analysis. To clarify this issue, structural analysis of Uba5 is required. This issue is currently under investigation in our laboratories. So far, most E1-like enzymes activate single species of UBL protein, although Atg7 is exception, which can activate both Atg8 and Atg12 (Mizushima *et al*, 1998; Tanida *et al*, 1999; Ichimura *et al*, 2000). A total of 10 E1-like enzymes can be identified in the human genome by computer analysis. Considering the limited number of E1-like proteins, it is possible that some E1-like proteins can activate a distinct set of UBL proteins. Whether or not Uba5 is capable of activating proteins other than Ufm1 remains to be clarified.

There are more than a dozen of E2 family genes in human genomes. In the budding yeast, 13 different E2s, namely Ubc1–Ubc13, have been documented and functionally characterized. Functionally, most of them catalyze the conjugation of ubiquitin, except that Ubc9 and Ubc12 are for SUMO and NEDD8/Rub1, respectively (Johnson and Blobel, 1997; Lammer *et al*, 1998; Osaka *et al*, 1998). In addition, in the autophagic pathway, Atg3 and Atg10 are both E2 enzymes for Atg8 and Atg12, respectively, but they do not have obvious sequence similarities to known Ubc's, except for a short region encompassing an active Cys residue (Shintani *et al*, 1999; Ichimura *et al*, 2000). Similarly, Ufc1 is a unique E2-like enzyme with no obvious sequence homology with other E2s, except approximately 10 amino-acid residues encompassing the active site Cys residue.

In assessing the biological roles of the Ufm1-modifying system, characterization of the target molecule(s) is of particular importance. Regarding this issue, we identified several putative proteins that are conjugated with Ufm1 in human HEK293 cells and various mouse tissues. It is noteworthy that the sizes of these bands (28, 38, 47 kDa) increase by 10 kDa, which is consistent with the size of Ufm1. Considering that several Ubl modifiers can attach to target proteins as a polymer, it is possible that these bands correspond to multi- or poly-Ufm1 conjugates. In fact, Ufm1 has six Lys residues. Whether Ufm1 is conjugated to several distinct proteins or multiple Lys residues in a single target or polymerized in a single Lys residue awaits future study. Unfortunately, we could not identify the protein, and detailed analysis of the cellular function of Ufm1 conjugation awaits future study. It was recently reported that Uba5 is induced by certain reagents that induce stress in the endoplasmic reticulum (ER), a so-called 'unfolded protein response' (Harding *et al*, 2003). However, we could not observe the induction of Uba5, Ufc1, and Ufm1 by treatment with various compounds known to induce ER stress in mammalian cells (data not shown). In addition, exposure to other stresses including high temperature or heavy metals also did not induce the appearance of obvious new conjugation band(s) of Ufm1, by immunoblot analysis. Further studies on the biological roles of the Ufm1 conjugation pathway are under investigation in our laboratories.

Materials and methods

DNA construction

The cDNA encoding human Uba5 was obtained by PCR from human liver cDNA with the Uba5-s5′ primer (5′-CGGAGGGATCCC CATGGCGGAGTCTGTGGAG-3′) and the Uba5-r3′ primer (5′-CAGTCCTCGAGCTACATATTCTTCATTTT-3′). It was then subcloned into pcDNA3 vector (Invitrogen, San Diego, CA). A point mutation for Cys at position 250 to Ser or Ala was generated by PCR-based site-directed mutagenesis. The Flag tag was introduced at the N-terminus of Uba5 or Uba5^{C250S}. Similarly, cDNA encoding human Ufm1 was amplified by PCR from human liver cDNA with the Ufm1-s5′ primer (5′-TTCCGGGATCCCCATGTCGAAGGTTTCCTTT-3′) and the Ufm1-r3′ primer (5′-AGTAGCTCGAGTTAACAACTTCCAA CACGAT-3′), and subcloned into pcDNA3 vector. The Flag, FlagHis, or Myc tags were introduced at the N-terminus of Ufm1. The HA tag was introduced at the C-terminus of Ufm1. The C-terminal deletion mutants of Ufm1 named Ufm1ΔC2 and Ufm1ΔC3, encoding amino acids 1–83 and 1–82, respectively, were generated by PCR. A point mutation for Gly at position 83 to Ala of Ufm1 and Ufm1ΔC2 (Ufm1^{G83A} and Ufm1ΔC2^{G83A}, respectively) was generated by PCR-based site-directed mutagenesis. The cDNA encoding human Ufc1 was obtained by PCR from human liver cDNA with the Ufc1-s5′ primer (5′-GCCCTGGATCCAGATGGCGGATGAAGCCACG-3′) and the Ufc1-r3′ primer (5′-TTCTCGAGTCATTGGTTGCATTTCTCTT-3′). It was then subcloned into pcDNA3 vector. A point mutation for Cys at position 116 to Ser or Ala was generated by PCR-based site-directed mutagenesis. The Flag tag was introduced at the N-terminus of Ufc1 and Ufc1^{C116S}. To express GST-fused Ufm1ΔC2, Ufm1ΔC3, Uba5, Uba5^{C250A}, Ufc1, and Ufc1^{C116A} in *E. coli*, these cDNAs were subcloned into pGEX-6p vector (Amersham Biosciences). All mutations mentioned above were confirmed by DNA sequencing.

Cell culture and transfection

Media and reagents for cell culture were purchased from Life Technologies (Grand Island, NY). HEK293 cells were grown in Dulbecco's modified Eagle's medium (DMEM) containing 10% fetal calf serum (FCS), 5 U/ml penicillin, and 50 μg/ml streptomycin. HEK293 cells at subconfluence were transfected with the indicated plasmids using Fugene 6 reagent (Roche Molecular Biochemicals, Mannheim, Germany). Cells were analyzed at 20–24 h after transfection.

Immunological analysis

For immunoblot analysis, cells were lysed with ice-cold TNE buffer (10 mM Tris–HCl, pH 7.5, 1% Nonidet P-40, 150 mM NaCl, 1 mM ethylenediaminetetraacetic acid (EDTA), and protease inhibitors) and the lysates were separated by SDS–PAGE (12% gel or 4–12% gradient gel) and transferred to a polyvinylidene difluoride (PVDF) membrane. Mouse monoclonal anti-Flag antibody (M2; Sigma Chemical Co., St Louis, MO), anti-HA antibody (F7; Santa Cruz Biotechnology, Santa Cruz, CA), and rabbit polyclonal anti-Myc antibody (N14; Santa Cruz) were used for immunodetection. Development was performed by the Western lighting detection methods.

For immunoprecipitation analysis, cells were lysed by 200 μl of TNE, and the lysate was then centrifuged at 10 000 *g* for 10 min at 4°C to remove debris. In the next step, 800 μl of TNE and 30 μl of M2-agarose (Sigma) were added to the lysate, and the mixture was mixed under constant rotation for 12 h at 4°C. The immunoprecipitates were washed five times with ice-cold TNE. The complex was boiled for 10 min in SDS sample buffer in the presence of β-mercaptoethanol to elute proteins and centrifuged at 10 000 *g* for 10 min at 4°C. The supernatant was subjected to SDS–PAGE, transferred to PVDF membrane, and analyzed by immunoblots with anti-Flag (M2) or anti-Myc (N14) antibody.

For purification of 6xHis-tagged proteins under denaturing conditions, cells were lysed by 1 ml of denaturing lysis buffer (8 M urea, 0.1 M NaH_2PO_4, and 0.01 M Tris–HCl, pH 8.0) in the presence of 20 mM *N*-ethylmaleimide as an inhibitor of isopeptidases, and the lysate was sonicated briefly and then centrifuged at 10 000 *g* for 10 min at room temperature to remove debris. Then, 30 μl of Ni-NTA Superflow (QIAGEN) was added to the lysate, and the mixture was shaken under constant rotation for 30 min at room temperature. The precipitates were washed five times with denaturing wash buffer (8 M urea, 0.1 M NaH_2PO_4, and 0.01 M Tris–HCl, pH 5.9). To elute proteins, elution buffer (8 M urea, 0.1 M NaH_2PO_4, and 0.01 M Tris–HCl, pH 4.5) was added to the complex, and the mixture was centrifuged at 10 000 *g* for 10 min at room temperature. The resulting supernatant was subjected to SDS–PAGE, transferred to PVDF membrane, and analyzed by immunoblots with anti-Flag (M2).

Freshly isolated tissues from mice were homogenized in lysis buffer (50 mM Tris–HCl, pH 7.5, 1% SDS, 5 mM EDTA, and 10 mM β-mercaptoethanol) using potter-Elvehjem homogenizer. The homogenate was centrifuged at 10 000 *g* for 10 min to remove debris. The resulting supernatant was subjected to SDS–PAGE, transferred to PVDF membrane, and analyzed by immunoblotting with anti-Ufm1 or preimmune serum. The anti-Ufm1 polyclonal antibody was raised in rabbits using the recombinant protein produced in *E. coli* as an antigen.

In vitro thioester formation assay

Recombinant GST-Ufm1ΔC2, GST-Ufm1ΔC3, GST-Uba5, GST-Uba5^{C250A}, GST-Ufc1, and GST-Ufc1^{C116A} (tagged N-terminally with GST) were produced in *E. coli* and recombinant proteins were purified by chromatography on glutathione sepharose 4B (Amersham Biosciences). After elution of proteins from the beads, the preparations were dialyzed against 50 mM BisTris (pH 6.5), 100 mM NaCl, 10 mM $MgCl_2$, and 0.1 mM DTT (reaction buffer). Most thioester formation reactions contained reaction buffer with 4 μg GST-Ufm1ΔC2 or GST-Ufm1ΔC3 and some of the following: 5 mM ATP, 2 or 0.2 μg GST-Uba5 or GST-Uba5^{C250A}, and 4 μg GST-Ufc1 or GST-Ufc1^{C116A}. Reactions were incubated for 30 min at 25°C and stopped by the addition of SDS-containing loading buffer either lacking reducing agent or containing 100 mM DTT, followed by a 10 min incubation at 37°C, SDS–PAGE (4–12% acrylamide gradient) and Coomassie brilliant blue staining.

Protein identification by LC–MS/MS analysis

The Uba5-associated complexes were digested with *Achromobacter* protease I and the resulting peptides were analyzed using a nanoscale LC–MS/MS system as described previously (Natsume *et al*, 2002). The peptide mixture was applied to a Mightysil-PR-18 (1 μm particle, Kanto Chemical) frit-less column (45 mm × 0.150 mm ID) and separated using a 0–40% gradient of acetonitrile containing 0.1% formic acid over 30 min at a flow rate of 50 nl/min. Eluted peptides were sprayed directly into a quadropole time-of-flight hybrid mass spectrometer (Q-Tof *Ultima*, Micromass, Manchester, UK). MS and MS/MS spectra were obtained in a data-dependent mode. Up to four precursor ions above an intensity threshold of 10 counts/s were selected for MS/MS analyses from each survey scan. All MS/MS spectra were searched against protein sequences of Swiss Prot and RefSeq (NCBI) using batch processes of Mascot software package (Matrix Science, London, UK). The criteria for match acceptance were the following: (1) When the match score was 10 over each threshold, identification was accepted without further consideration. (2) When the difference of score and threshold was lower than 10, or when proteins were identified based on a single matched MS/MS spectrum, we manually confirmed the raw data prior to acceptance. (3) Peptides assigned by less than three y series ions and peptides with +4 charge state were all eliminated regardless of their scores.

Immunofluorescence

HeLa cells grown on glass coverslips were fixed in 4% paraformaldehyde (PFA) in PBS for 15 min, and permeabilized with 0.2% (vol/vol) Triton X-100 in PBS for 30 min. After permeabilization, the cells were blocked for 30 min with 5% (vol/vol) normal goat serum in PBS, incubated for 1 h at 37°C with anti-Ufm1 serum or preimmune serum, washed with PBS, and incubated for 30 min with Alexa 488 nm anti-rabbit antibodies (Molecular Probes). The coverslips were washed and mounted on slides. Fluorescence images were obtained using a fluorescence microscope (DMIRE2; Leica) equipped with a cooled charge-coupled device camera (CTR MIC; Leica). Pictures were taken using Leica Qfluoro software (Leica).

Acknowledgements

We thank T Mizushima (Nagoya University) for the computer-assisted structural modeling of human Ufm1. This work was supported in part by Grants-in-Aid from the Ministry of Education, Culture, Sports, Science and Technology of Japan.

References

Bonifacino JS, Weissman AM (1998) Ubiquitin and the control of protein fate in the secretory and endocytic pathways. *Annu Rev Cell Dev Biol* **14**: 19–57

Cort JR, Chiang Y, Zheng D, Montelione GT, Kennedy MA (2002) NMR structure of conserved eukaryotic protein ZK652.3 from *C. elegans*: a ubiquitin-like fold. *Proteins* **48**: 733–736

D'Cunha J, Knight Jr E, Haas AL, Truitt RL, Borden EC (1996) Immunoregulatory properties of ISG15, an interferon-induced cytokine. *Proc Natl Acad Sci USA* **93**: 211–215

Furukawa K, Mizushima N, Noda T, Ohsumi Y (2000) A protein conjugation system in yeast with homology to biosynthetic enzyme reaction of prokaryotes. *J Biol Chem* **275**: 7462–7465

Glickman MH, Ciechanover A (2002) The ubiquitin-proteasome proteolytic pathway: destruction for the sake of construction. *Physiol Rev* **82**: 373–428

Harding HP, Zhang Y, Zeng H, Novoa I, Lu PD, Calfon M, Sadri N, Yun C, Popko B, Paules R, Stojdl DF, Bell JC, Hettmann T, Leiden JM, Ron D (2003) An integrated stress response regulates amino